Lehrstuhl für Hochfrequenztechnik
Technische Universität München
Prof. Dr.-Ing. Thomas Eibert

Master's thesis

Analysis of Influences on Antenna Radiation Patterns by Conducting Environments for the Development of Vehicle Antennas

Vicente A. Fuertes Pals

26.07.2013

Supervisor: Dipl.-Ing. Marina S. L. Mocker
Beginning of the thesis: 08.10.2012
End of the thesis: 26.07.2013

To the memory of my grandmother

Forgive me for not having been at your side in the worst day of your life...
08-07-2013

I love you

Contents

Symbols	Units	Meaning
f	GHz	Frequency
w	GHz	Angular frequency
c	m/s	Light velocity
l	mm	Antenna length
λ	mm	Wavelength
E	V/m	Electric field
H	A/m	Magnetic field
D	C/m^2	Electric field displacement
B	Wb/m^2	Magnetic field flux
J	A/m^2	Current density
A	Wb/m	Vector potential
P	W/m^2	Radiation power density
K	W/Ω	Radiation intensity
W_{rad}	W	Radiated power
W_{dlv}	W	Power delivered to an antenna
t		Power radiation pattern
d		Field radiation pattern
Rd	mm	Wire radius
Hd	mm	Half wire length
Hp	mm	Plane height
Hw	mm	Plane width
Tp	mm	Plane thickness
Rp	mm	Circular plane radius
Kd	mm	Distance between the two half wires of the dipole
Kp	mm	Distance between plane and dipole
L	mm	Dipole length
D	dB	Directivity
G	dB	Gain

Constants	Value	Meaning
Kd	$\lambda/100$	Distance between the dipole wires
Hd	$\lambda/4$	Half length of the dipole

Abbreviations	Meaning
PEC	Perfect Electric Conductor
CST	Computer Simulation Technology
EM	Electromagnetic
MWS	Microwave Studio
GTD	Geometrical Theory Diffraction
GO	Geometrical Optics
GSM	Global System for Mobile Communications
GPS	Global Positioning System
FEA	Finite element analysis
NASA	National Aeronautics and Space Administration
3D	3 Dimensions
GNSS	Global Navigation Satellite System
T	Time Domain Solver
F	Frequency Domain Solver
EMCoS	Electromagnetic Compatibility Operating Systems
HFSS	High Frequency Structural Simulator

Greek Symbols	Units	Meaning
ρ	C/m^3	Charge density
ε	F/m	Permittivity
μ	H/m	Permeability
σ	S/m	Electric conductivity
Φ	V	Electric potential
η	Ω	Characteristic impedance of the medium
θ	Degrees	Theta angle
ϕ	Degrees	Phi angle
$\Delta\phi$	rad	Phase difference
Ω	Sr	Solid angle

1 Introduction

In 19th century wireless communications found its beginning with the developments of Marconi [1] on long distance radio transmission. The steady progress in its state of the art leads to an increasing number of applications and an increase in its importance. This trend is also true for the developments in the vehicle sector. In vehicles of today a huge number of radio frequency services are integrated yet. Some examples are radio, telephone and the global positioning system for navigation [2]. The number of required antennas will increase as there is a demand for new services like Long Term Evolution and car to car communication. This will lead to an integration of twenty antennas or more in each vehicle. For every single antenna a position and a behaviour has to be defined and optimized.

A further trend in the vehicle industry is the reduction of available development time. To achieve the aim of reduced development cost and time, a more efficient way to create new antenna concepts, is to use simulations. With virtual test drive simulations, measurement campaigns can be replaced completely. For antenna simulations many commercial tools like CST MWS [3], EMCoS [4] or ANSYS HFSS [5] for high-frequency problems are available. CST MWS is a specialist tool for the 3D EM simulation of high frequency components. It enables the fast and accurate analysis of high frequency devices such as antennas or filters. EMCoS Antenna VirtualLab is a powerful program package especially suited for antenna calculations. The program package allows in a very convenient way to design and model complicated antenna structures, calculate them accurately and easily process the results. ANSYS HFSS is a software for simulating 3D electromagnetic fields. It offers multiple solver technologies based on finite element, integral equation or advanced hybrid methods to solve a wide range of applications.

Many important characteristics like reflection parameters, far-field patterns or surface currents can be simulated with them. Usually the reflection parameter and far-field pattern of an antenna in ideal environment are optimized. Mounting the antenna on a vehicle and thus taking into account the direct environment changes those parameters. The best solution for the optimization of antennas on vehicles would be the import of the whole vehicle structure but as the vehicle is large in respect to the wavelength, the simulation is very time consuming and takes many resources.

For this purpose, CST MWS is used to gain knowledge about the influence of such reductions. As the conducting structures get smaller, several effects due to the discontinuities appear and need to be investigated. For example discontinuities are, as the corners of a structure produce diffracted rays [6][7].

The study of such effects allows the possibility to gain general knowledge about the influence of direct conducting environment on an antenna. This allows to know which behaviour can be expected by changing the vehicle structure and thus save time by starting the right sim-

ulations. Additionally by using the right reductions of the conducting structure, the required time to achieve good simulation results becomes shorter and this means less development costs. Therefore the conducting environment should to be reduced to find a compromise between accuracy and computational effort.

2 Antenna radiation fundamentals

Antennas is a transducer between guided and free-space energy. Therefore, antennas transform guided energy to radiated electromagnetic waves. To understand the behaviour of an antenna, several parameters definitions are necessary to describe important effects of antennas and help to gain better knowledge about the variables which are commonly used to evaluate the performance of it. In addition, the majority of them are used in order to explain the simulation results. Therefore, these definitions are introduced for better understanding of the final results of this research work and are going to provide a solid background of the topic.

The simulation tool used in this research work is able to calculate the antenna parameters used in this work. Besides the common values as directivity or gain, there is one more that cannot always be clearly calculated. This parameter is called phase center and the simulation software provides a tool to calculate it. Thus, in this chapter, the phase center is introduced and the calculation viability of it with the software tool is analysed.

2.1 Radiation pattern

From a practical point of view, the antennas are described from a set of variables which determine its features and adequacy to a certain application. The antenna is a transducer element, that is connected to a circuit and emits waves, we could distinguish two kind of variables. On one side there are those that describe the antenna from the radiant point of view, for example gain or polarization. On the other side there are those that are used to characterise the antenna as an element of a circuit, for example the impedance or effective area.

The radiation pattern is the most characteristic value of an antenna. It is defined as a graphical representation of the radiation properties as a function of space coordinates [6]. Normally, the radiation pattern is determined in the far-field or Fraunhofer region, see next section, and is represented as a function of the spherical coordinates θ and ϕ, as shown in Figure 2.1. This representation is typically 3D quantities involving the variation of the field or the variation of the power proportional to the field square. Often either the field or the power pattern normalized with respect to their maximum value are plotted in dB.

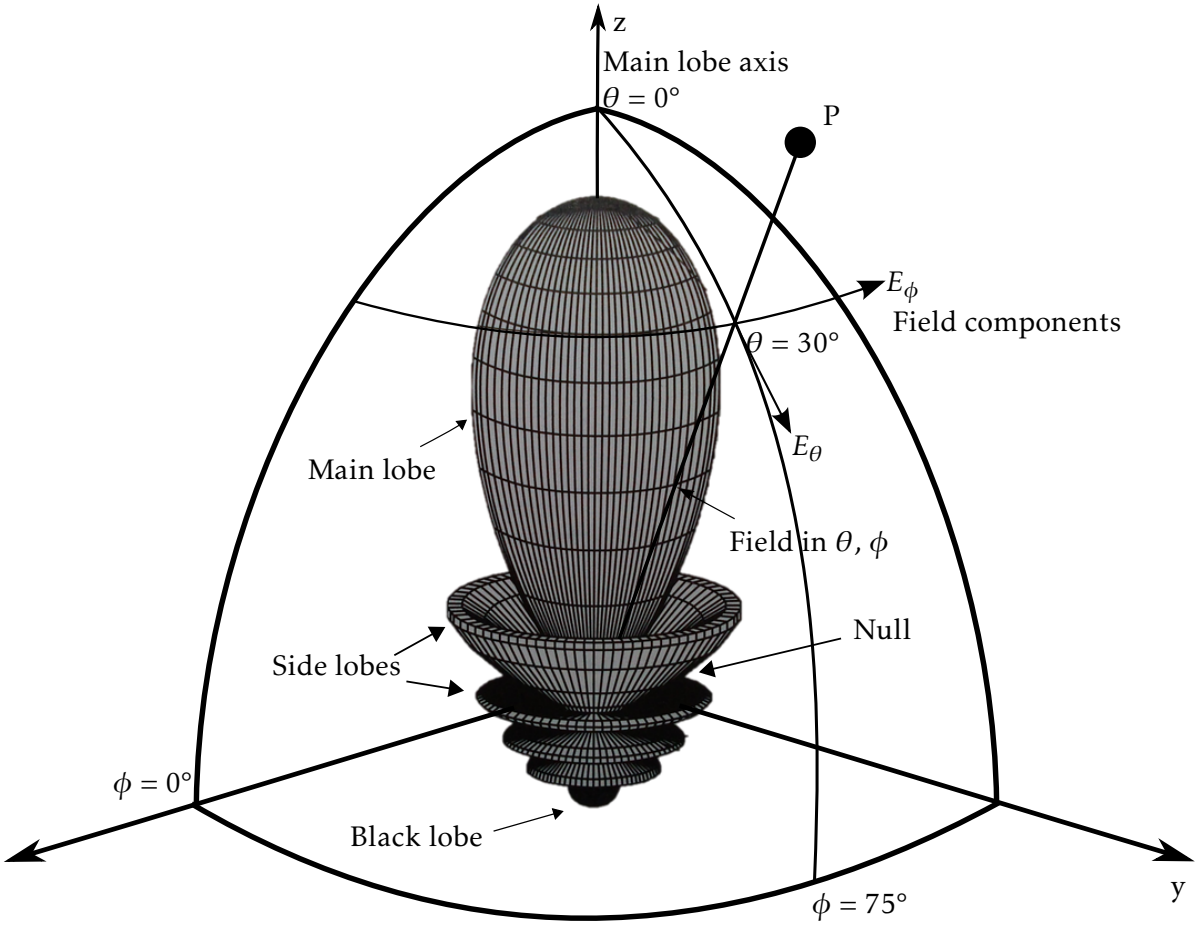

Figure 2.1: 3D field pattern of a directional antenna with its maximum of the radiation pattern at $\theta = 0°$ or in Z direction [8].

As shown in Figure 2.1, the radiation pattern is formed by main, side and black lobes. On the one hand, the main lobe, which is oriented along the Z axis, has a larger lobe than the others. On the other hand, the side lobes usually represent unwanted radiation in undesired directions. Finally, the side lobe located in the opposite direction of the main lobe is called black lobe. The nulls separate the lobes and are located in angles where the radiation falls to zero. However, these radiation pattern calculations are not easy to solve in complex problems, for example when not only an antenna is considered. Therefore, several simulation programs, for example CST MWS [3], are available to calculate and plot these radiation patterns.

The antenna radiation pattern can be described from the four Maxwell equations[9]. When the sources vary harmonically with the time, the electromagnetic equations and their solutions are simplified using for that a phasorial notation, so that the derivatives respect to the time are transformed in products by the factor jw. The equations below show the Maxwell equations with electric current sources and assuming homogeneous space [6][10].

$$\nabla \times \overrightarrow{H} = \overrightarrow{J} + jw\varepsilon \overrightarrow{E} \qquad \textbf{Ampère's law} \qquad (2.1)$$

$$\nabla \times \overrightarrow{E} = -jw\mu\overrightarrow{H} \qquad \textbf{Faraday's law} \qquad (2.2)$$

$$\nabla \cdot \overrightarrow{D} = \rho \qquad \textbf{Gauss's law} \qquad (2.3)$$

$$\nabla \cdot \overrightarrow{B} = 0 \qquad \textbf{Gauss's law for magnetic fields} \qquad (2.4)$$

Regarding the general expression of the Maxwell equations, the Ampere's law idea is that if the electric flux through any surface bounded by a path changes over time, a magnetic field along the path is produced. If the magnetic flux through a surface changes, an electric field along the boundary of that surface as says Faraday's law is induced. Moreover, the Gauss's law shows that if there is a real or imaginary closed surface of any size and shape and there is no charge inside the surface, the electric flux through the surface must be zero. Additionally, if there is a real or imaginary closed surface of any size or shape, the total magnetic flux through that surface must be zero, as says Gauss's law for magnetic fields. Each of the four equations is very important for itself. However, the achievement of Maxwell was something beyond the synthesis of theses laws. It was by considering these laws in combination with the Ampere's law that let him to reach the goal of developing a theory of electromagnetism. With the Maxwell equations handling and two important theorems of vector calculus, the divergence and Stoke's theorem, is possible to reach the wave equation as shown in equation 2.5, where $\overrightarrow{A}$ is the vector potential defined in equation 2.7 and $\overrightarrow{J}$ is the current density [6][10].

$$\nabla^2\overrightarrow{A} + k^2\overrightarrow{A} = -\mu\overrightarrow{J} \qquad (2.5)$$

The previous wave equation can be taken apart in three scalar equations, corresponding to each one of the Cartesian components of the vector.

$$\begin{aligned} \nabla^2 A_x + k^2 A_x &= -\mu J_x \\ \nabla^2 A_y + k^2 A_y &= -\mu J_y \\ \nabla^2 A_z + k^2 A_z &= -\mu J_z \end{aligned} \qquad (2.6)$$

From the wave equation it is possible to obtain the vector potential. In some cases is also defined another parameter which is included in the vector potential $\overrightarrow{A}$ and is known as radiation vector $\overrightarrow{N}$ as shown in equation 2.7. In addition, with the vector potential $\overrightarrow{A}$, the expression for the electric field $\overrightarrow{E}$ can be obtained as shown in equation 2.8.

$$\overrightarrow{A} = \frac{\mu e^{-jkr}}{4\pi r} \iiint_{v'} \overrightarrow{J}(\overrightarrow{r'}) e^{jk\overrightarrow{r'}\cdot\hat{r'}} dv' = \frac{\mu e^{-jkr}}{4\pi r}\overrightarrow{N} \qquad (2.7)$$

$$\overrightarrow{E} = -jw\overrightarrow{A} = -jw(A_\theta\hat{\theta} + A_\phi\hat{\phi}) \tag{2.8}$$

It can also be expressed in spherical coordinates with the radiation vector $\overrightarrow{N}$ as shown in equation 2.9, where N_θ, N_ϕ are the spherical components of the radiation vector $\overrightarrow{N}$. The radiation vector $\overrightarrow{N}$ and in consequence the electric field $\overrightarrow{E}$ are always computed in the far-field or Fraunhofer region, see Section 2.2. The distance R from the antenna where the far-field region is considered, corresponds to a R equal to $2D^2/\lambda$. From this distance R, the electric field is no longer dependent on the distance R and it only depends on θ and ϕ values.

$$\overrightarrow{E} = -jw\frac{\mu}{4\pi}\frac{e^{-jkr}}{r}[N_\theta\hat{\theta} + N_\phi\hat{\phi}] \tag{2.9}$$

Once the electric field is defined, the radiation pattern d [8] is obtained dividing the electric field module by the maximum electric field module as shown in equation 2.10.

$$d(\theta,\phi) = \frac{|\overrightarrow{E}(\theta,\phi)|}{|\overrightarrow{E}_{max}(\theta,\phi)|} \tag{2.10}$$

The radiation pattern is often expressed in dB with the following conversion $d(\theta,\phi)$ [dB] equal to $20\log(d(\theta,\phi))$.

2.2 Regions of the radiated fields

The characteristics of the electromagnetic field produced by an antenna differs depending on the distance from where it is observed. The space surrounding an antenna can be divided into three different regions: reactive near-field, radiating near-field (Fresnel region) and far-field (Fraunhofer region) as shown in Figure 2.2[6].

The reactive near-field region can be defined as the part of the near-field region immediately surrounding the antenna wherein the reactive-field predominates. The reactive field means the nature of the field around the antenna is sensitive or reacts to electromagnetic absorption. The outer boundary of this region is normally assumed to exist at a distance R_1 from the antenna surface given by

$$R_1 < 0.62\sqrt{l^3/\lambda} \tag{2.11}$$

where D is the length of the antenna as shown in Figure 2.2 and λ is the wavelength. However, for a very short radiator, the outer boundary is normally taken to exist at a distance of $\lambda/2\pi$ from the antenna surface.

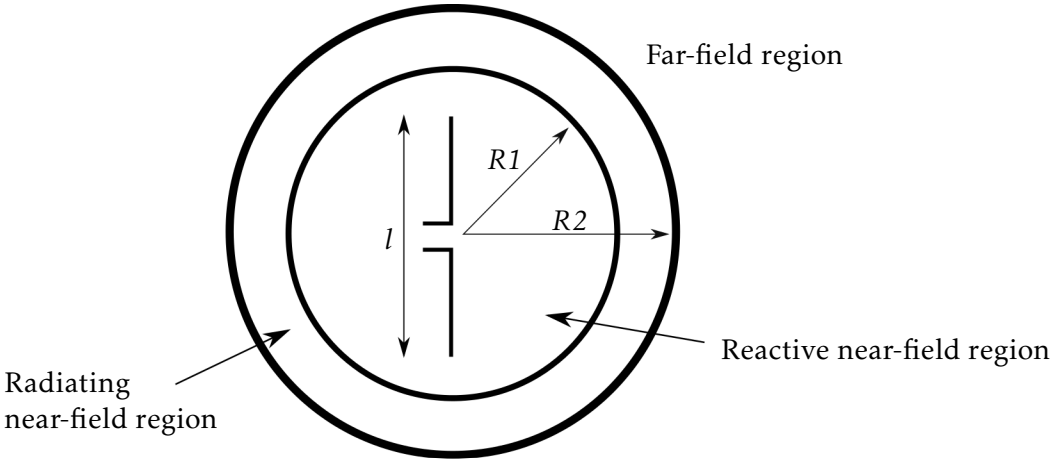

Figure 2.2: Field regions of an antenna, where l is the antenna length [6].

The radiating near-field or Fresnel region can be defined as the region of an antenna field between the reactive near-field region and the far-field region wherein radiated fields predominate and the angular field distribution is dependent upon the distance from the antenna. The inner boundary is normally assumed at a distance R_1 as shown in equation 2.11 and the outer boundary at a distance R_2 as shown in equation 2.12. In case the antenna has a maximum length which is not large enough in comparison to the wavelength, it is possible that the region does not exist.

$$R_2 < 2l^2/\lambda \tag{2.12}$$

Finally, the far-field region can be defined as the region of an antenna field where the angular field distribution is independent from the distance to the antenna. If the antenna has a maximum covering entirely the length l, with $l > \lambda$, the far-field region can be assumed to exist at distances greater than R_2 as shown in equation 2.12. In this region, the field components are in essence transverse and the angular distribution is independent of the radial distance where the measurements are made. The inner boundary is normally taken at a distance R_2 as shown in equation 2.12 and the outer one at infinity as shown in Figure 2.2.

The amplitude pattern of an antenna changes in shape due to the fact that the fields vary in magnitude and phase by changing the observation distance from the reactive near-field to the far-field. An example of an antenna shape progression respect to the largest length l, is shown in Figure 2.3. It shows the progression of a wave along the different regions. The radiated wave starts in the reactive near-field region and finishes in the far-field region as a planar wave.

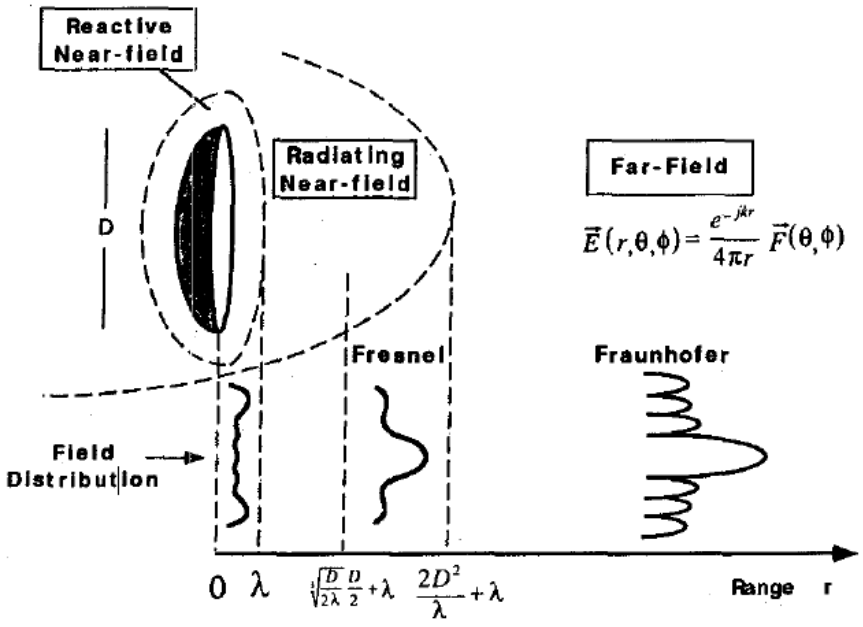

Figure 2.3: Wave propagation in reactive near-field, radiating near-field and far-field regions [11].

2.3 Gain and directivity

Directivity $D(\theta,\phi)$ and gain $G(\theta,\phi)$ [6][8] are two important parameters of an antenna. However it is necessary to define several variables to understand the directivity and gain definition. These parameters are the radiation power density $\overrightarrow{P}(\theta,\phi)$ and the radiation intensity $\overrightarrow{K}$.

The radiation power density $\overrightarrow{P}$ is defined as the power per surface unit in a particular direction and it decreases with the distance by $1/r^2$. Therefore, this parameter indicates the total value of power within a certain area and a particular distance. The units are watts per square meter and it can be calculated from the effective values of the fields [12] as

$$\overrightarrow{P}(\theta,\phi) = \mathrm{Re}[\overrightarrow{E}(\theta,\phi)\times\overrightarrow{H}^{*}(\theta,\phi)] \tag{2.13}$$

The relation between the electric and the magnetic field module is the characteristic impedance of the medium given by

$$\eta = \frac{|\overrightarrow{E}(\theta,\phi)|}{|\overrightarrow{H}(\theta,\phi)|} \tag{2.14}$$

Thus, the radiation power density can also be calculated from the components of the electric field [12] as shown in equation 2.15. As it is referred to the Fraunhofer region the field is only dependent on the θ and ϕ values. The relation between radiation intensity $\overrightarrow{K}(\theta,\phi)$

and radiation power density $\overrightarrow{P}(\theta,\phi)$ is given by $\overrightarrow{K}(\theta,\phi)$ equal to $\overrightarrow{P}(\theta,\phi)r^2$. Therefore, the radiation density is the power radiated from an antenna per unit solid angle Ω. It is also associated to the far-field region and is independent from the distance.

$$\overrightarrow{P}(\theta,\phi) = \frac{|\overrightarrow{E}|^2}{\eta} = \frac{|E_\theta|^2 + |E_\phi|^2}{\eta} \tag{2.15}$$

In addition, the power radiation pattern t of an antenna can be obtained from the radiation power density $\overrightarrow{P}(\theta,\phi)$ as

$$t(\theta,\phi) = \frac{|\overrightarrow{P}(\theta,\phi)|}{|\overrightarrow{P}_{max}(\theta,\phi)|} = d(\theta,\phi)^2 \tag{2.16}$$

Both equations of the diagram pattern, equation 2.10 and 2.16 are valid as t is the power radiation pattern and d is the field radiation pattern and the relation between field and power is equal to the square of the field. Finally, the radiated power can be obtained by integrating the radiation intensity $\overrightarrow{K}(\theta,\phi)$ within a sphere which contains the antenna due to the fact that in the far-field region the component $\overrightarrow{E}(r)$ of the electric field is assumed to be small. Therefore, the radiated power can be computed as the total radiation intensity over the entire solid angle of 4π [6] as shown in equation 2.17, where $d\Omega$ is equal to an element of solid angle, $d\Omega$ equal to $\sin\theta d\theta d\phi$.

$$W_{rad} = \int_0^{2\pi}\int_0^{\pi} K(\theta,\phi)d\Omega \tag{2.17}$$

As commented before, the radiation intensity is related to the radiation power density as $K(\theta,\phi) = P(\theta,\phi)r^2$, therefore the radiated power W_{rad} can be also computed as

$$W_{rad} = \int_0^{2\pi}\int_0^{\pi} P(\theta,\phi)r^2 d\Omega. \tag{2.18}$$

Considering the previous parameters, the directivity $D(\theta,\phi)$ of an antenna is defined as the relation between the radiation power density $\overrightarrow{P}(\theta,\phi)$ in a particular distance and direction, and the radiation power density variable that an isotropic antenna would radiate at the same distance as shown in Figure 2.4. An isotropic antenna is considered theoretically as a lossless and omnidirectional radiator. This means that the radiation power density of an isotropic antenna is the radiated power W_{rad} divided by the surface area of a sphere. In both cases the same radiated power W_{rad} is considered, therefore the directivity indicates how much radiation power density is produced by a particular antenna in respect to the isotropic one.

The energy is not radiated equally in all directions but is gathered in some of them. The directivity $D(\theta,\phi)$ of an antenna is normally expressed in dB and is given by

$$D(\theta,\phi) = \frac{P(\theta,\phi)}{P_{isotropic}} = \frac{P(\theta,\phi)}{\frac{W_{rad}}{4\pi r^2}} \tag{2.19}$$

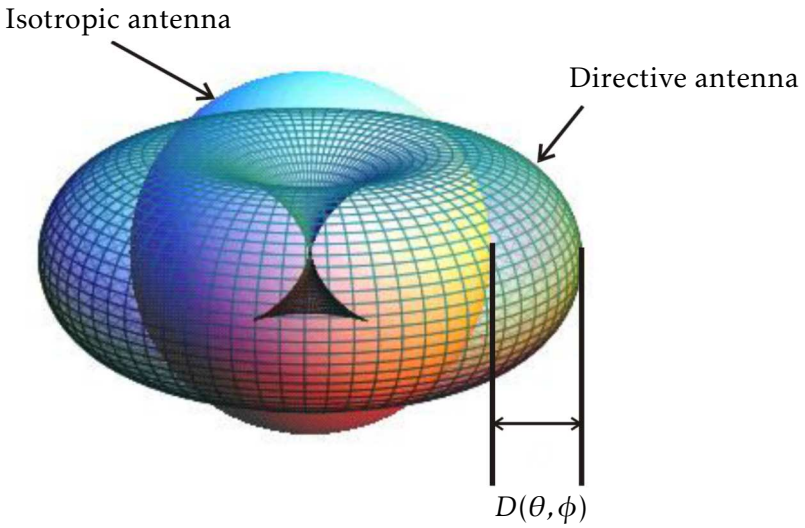

Figure 2.4: Visual interpretation of $D(\theta,\phi)$ [12].

A real antenna does not radiate all the delivered power to it because it is not ideal as shown in Figure 2.5. In case of the gain $G(\theta,\phi)$, it takes into account the loss between the delivered power W_{dlv} and radiated power W_{rad}, therefore now the radiated power W_{rad} is substituted by the power delivered W_{dlv} to the antenna. This way the gain describes the comparison between radiated power of our antenna and the radiated power of an isotropic antenna without losses, considering the same delivered power.Finally, the antenna gain is defined as

$$G(\theta,\phi) = \frac{P(\theta,\phi)}{\frac{W_{dlv}}{4\pi r^2}}. \tag{2.20}$$

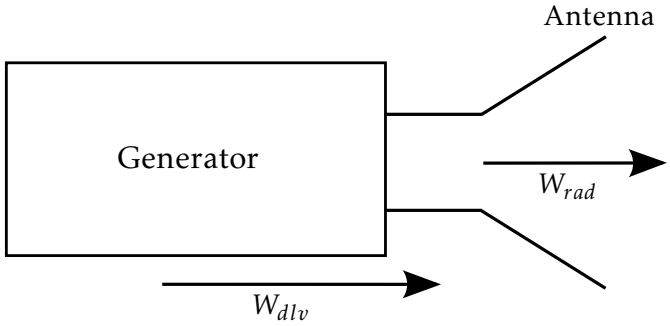

Figure 2.5: Power relation of an antenna [12].

2.4 Polarization

The electromagnetic field is a vectorial magnitude that varies with space and time. Hence, the polarization of a wave describes the temporal variation of the electric field vector for a given direction.

To simplify the definition, a planar wave that travels in the $\hat{z}$ direction is considered. Therefore, the instantaneous field of a plane wave travelling in this direction can be written as

$$\overrightarrow{E}(z,t) = \hat{x}E_x(z,t) + \hat{y}E_y(z,t) \tag{2.21}$$

The instantaneous field for harmonic variations, e^{jwt}, is given by

$$\begin{aligned} E_x(z,t) &= E_x cos(wt - kz + \phi_x) \\ E_y(z,t) &= E_y cos(wt - kz + \phi_y) \end{aligned} \tag{2.22}$$

where E_x and E_y are the maximum magnitudes of the x and y components respectively and $E_x e^{j\phi_x}$ and $E_y e^{j\phi_y}$ the phasors that define each one of the electric field components [12]. The projection of the vector $\overrightarrow{E}(z,t)$ in the XY plane describes an ellipse known as *polarization ellipse* as shown in Figure 2.6. The phasor of the total field is written as

$$\overrightarrow{E} = \hat{x}E_x e^{j\phi_x} + \hat{y}E_y e^{j\phi_y} \tag{2.23}$$

and defines the wave.

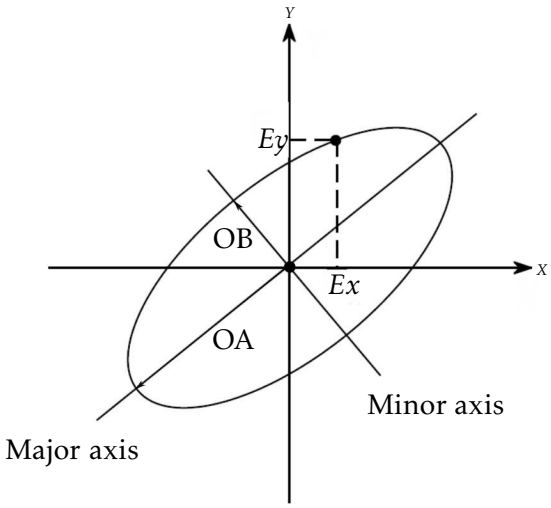

Figure 2.6: Polarization ellipse [12].

Nevertheless, several particular cases can be distinguished depending on the magnitudes or phase differences ($\Delta\phi = \phi_y - \phi_x$) between the two orthogonal components of the electric field $\overrightarrow{E}(\theta,\phi)$. These particular cases are linear, circular and elliptical polarization. In this work, a linear polarization is generated due to the antenna characteristics [6][8].

If a wave is linear polarized, it is necessary that one of both field magnitudes is zero, $E_x = 0$ or $E_y = 0$. The time-phase difference between both components has to be

$$\Delta\phi = \phi_y - \phi_x = n\pi, \quad \text{where} \quad \text{n} = 0,1,2,3,4... \tag{2.24}$$

This is the extreme case of an ellipse in which one of its semiaxis is zero. Some possible associated phasors could be $\overrightarrow{E} = \hat{x}$ or $\overrightarrow{E} = \hat{y}$.

Finally, a circular polarization can be achieved when the magnitudes of both components are equal and the time-phase difference is odd multiples of $\pi/2$. Other combinations of amplitudes or phase differences produce an elliptical polarization.

2.5 Phase Center

The phase center of an antenna can be defined as the apparent place or point from which a signal emanates. The radiated fields measured on the surface of a sphere whose center coincides with the phase center have the same phases [6]. On the contrary, there is no real antenna which is small enough to be a source point, so the radiation emanates from a larger area. In the majority of cases the phase center seems to be in different positions of an area depending on the observation point. Nevertheless, in some specific antenna systems this reference point can be found such that the phase of the electric field maintains the same value

for the different angles (θ and ϕ are constant) or nearby. In addition, when the variation of the phase center position is sufficiently small, that point can be considered as the phase center.

The interesting point about the phase center is to compute exactly the source point of an antenna. This is of special interest if the position of an antenna has to be estimated exactly at one point. For example with Ray-tracing which is a technique for generating an image by tracing the path of light through pixels in a image plane this is the case. Ray-tracing is used to approximate the propagation of electromagnetic fields and their interaction with objects. The receiving antenna is defined by a point and the rays which arrive close by, are propagated towards this point to compute the received signal. For this reason, the phase center estimation could be very useful ray-tracing problems.

After the definition of the phase center and regarding to the calculation methods of it, there are several papers published on the subject of phase center determination. However, these methods are not general but they are more specific, as for example phase center calculation for horn antennas. The phase center calculation methods could be classified in different groups, for example phase calculation for horn antennas [13] [14], for GNSS applications [15], for microwave antennas [16] or radio antennas for aircraft and aerospace vehicles [17].

In this research work, the antenna under study is omnidirectional and a specific procedure for this kind of antenna could not found. However, the used software CST MWS [3], has a tool available for phase center calculations. It is possible to plot the phase center representation as well as the radiation pattern. The first problem found was that in almost all simulations, CST was not able to plot the phase center due to the fact that the supposed phase center was outside the program working area. Additionally, CST provides the coordinates of the phase center and the standard deviation Sigma which shows how much variation or dispersion exists from the average or expected value. It indicates whether the phase calculation is far from the average or not and in consequence if the result is wrong or not. Almost always Sigma was high which indicates that the result is not of good quality.

The phase center in CST is calculated from phase values in two planes for a constant reference distance. One plane is defined by the polarization vector y and z axis called E-Plane. The other plane is defined by the x and z axis perpendicular to the E-Plane, called H-Plane. Depending on the selected plane the phase center will be calculated for the E-Plane, H-Plane or for both planes. If both planes are calculated, the phase center location is averaged afterwards. In Figure 2.7 an example of the phase center calculations in CST is shown. In this case, the phase center is plotted as the coordinate of it is within the working area but the extremely Sigma indicates that the value is incorrect. The problem is that the phase center computation in CST MWS is only intended for directional antennas as for example horn antennas. For these reasons, there was no possibility to calculate the phase center for the antenna used in this research work, therefore the phase center could not be considered.

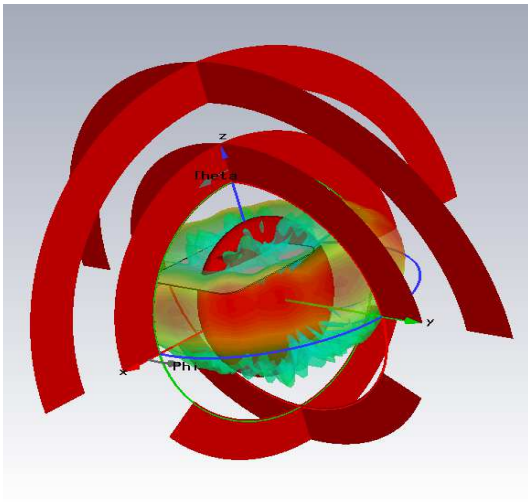

(a) Phase center representation in CST

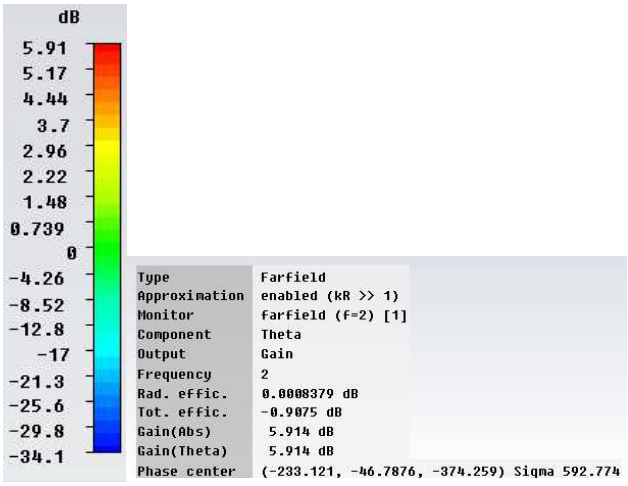

(b) Legend and phase center parameters

Figure 2.7: Example of phase center representation in CST.

3 Theoretical background for radiation pattern analysis

There are several procedures to analyse the influences on the antenna radiation pattern when the antenna is near to conducting environments. In this chapter theoretical procedures are going to be introduced to understand the behaviour of an antenna closed to an infinite conducting plane and the effects which are produced when the conducting plane is finite.

3.1 Image Theory

Image theory is a methodology to analyse an antenna which is located close to conducting environments. The method consists in simplifying the problem substituting the conducting plane by an additional antenna which allows to compute the radiation pattern easier. Image theory shows that it is possible to analyse the conducting environment as an antenna with the reflection law.

In this work antenna problems with conducting environment are going to be studied. The presence of an object, for example a vehicle structure near an antenna, can alter the radiation properties of the whole antenna system. Any wave travelling towards the structure undergoes a reflection due to it. In case of an infinite perfect electric conductor (PEC) object an image theory procedure can be introduced and it can help to understand the effects which can be observed in the next chapters. In reality, the objects that influence the radiation pattern are always finite but image theory can be applied to objects sufficiently large as well.

To simplify the analysis of image theory, a flat, infinite and perfect electric conductor (PEC) is assumed. The performance of an antenna close to an infinite conducting plane can be regarded as a real antenna above the conductor plane and a virtual antenna below it. The virtual antenna is located at the same distance from the conducting plane as the real antenna, as shown in Figure 3.1. Every reflected wave of the real antenna is joined at one point with the directed wave. If the reflected wave is extended downward from the plane, casually all the waves are joined in another point where the virtual antenna is. Therefore, it can be assumed that the real and virtual antenna radiate the same field from above and from below the conductor plane.

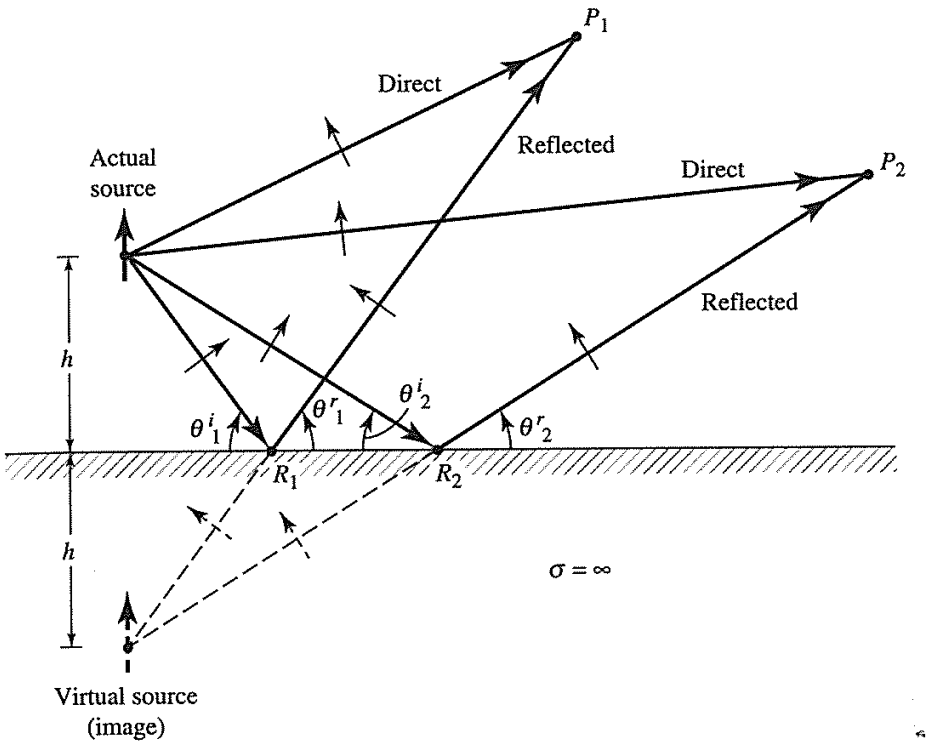

Figure 3.1: Vertical antenna above a flat, infinite PEC [6].

In Figure 3.1, there is shown the actual source as the antenna above the plane and the virtual source as the virtual antenna below the plane as well as the direct and reflected rays. The energy from the actual source is radiated in all directions determined by its medium properties. There is a direct wave that propagates downwards the observation point P_1. A second wave towards the conductor plane with an incident angle θ_1^i. According to the reflection law, which implies a reflection angle θ_1^r equal to the incident one (θ_1^i=θ_1^r), the energy travels always in straight lines and along the shortest paths in case of homogeneous media. Therefore, as a flat PEC plane is considered, the incident wave is completely reflected and meets the direct wave at the same point P_1. The same effect can be observed on observation point P_2.

Extending the reflected waves of both observation points downwards the conductor plane, they are joined in one point under the conductor plane as described before. This point is located at the same distance from the conductor plane as the actual source, resulting in the virtual source, which can also be called image. To hold in this boundary conditions, the virtual source must to be located vertically and polarized in the same direction as the actual source as shown in Figure 3.2. The effect of the induced currents and charges on the conductor plane can be analysed replacing the conductor plane by its charges and currents, as shown in Figure 3.2. This procedure is going to be studied in Section 5.2 to prove its validity and to show how the radiation pattern changes due to an infinite conducting environment.

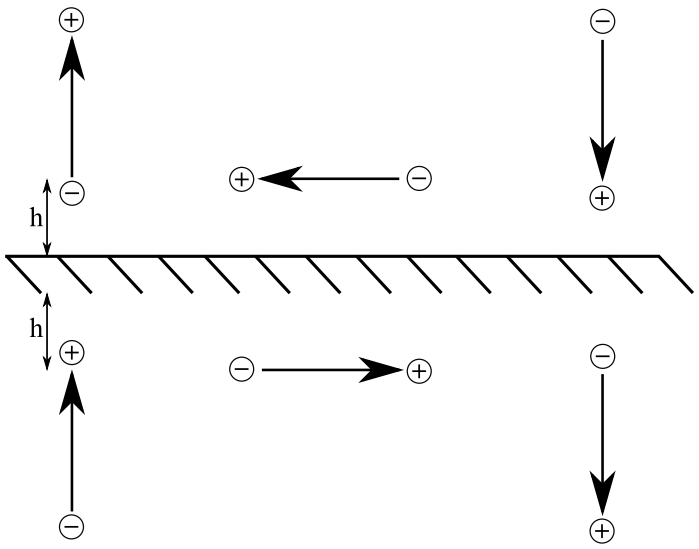

Figure 3.2: Electric sources and their images near to a PEC plane [12].

In case of finite conducting environments, additional effects occur due to the fact that a finite structure has discontinuities like edges or corners. When a discontinuity is present, the reflection law is no longer sufficient.

3.2 Geometrical Theory Diffraction

As commented in the previous section, infinite conductor planes are not realistic. In reality, they are finite and sometimes very large so that they can be approximate as an infinite plane. Therefore, in case of finite conductor planes, the radiation of an antenna can be modified by the limited size of it and some characteristics as impedance or current distribution are also influenced. In this particular case, the radiation characteristic undergoes big changes especially in the regions where its intensity is quite low due to the corners and edges of the conductor plane.

To solve this problem, the *Geometrical Theory of Diffraction* (GTD) [18] is introduced. The GTD is a method to calculate the diffracted waves due to the discontinuities of a finite structure. When a wave arrives to a corner or edge, the incoming ray is diffracted in many rays so that each ray contributes to the radiation pattern. The GTD is usually used when the object under study is large compared to the antenna and is an extension of *Geometrical Optics* (GO), where direct and reflected rays can be considered. The diffracted rays are yielded when the object surface, for example a finite conducting plane, has discontinuities like edges or corners. The phase of a diffracted ray is equal to the product of the optical length and the phase value of the medium in which the ray is propagating. The amplitude is determined by the amplitude of the incident ray and a diffraction coefficient [6].

In general, the total electromagnetic field is resulting from the radiation of the antenna itself and the reflected and the diffracted rays. The diffraction mechanism [19][20] at a finite

conducting plane with an antenna radiating close to it is shown in Figure 3.3.

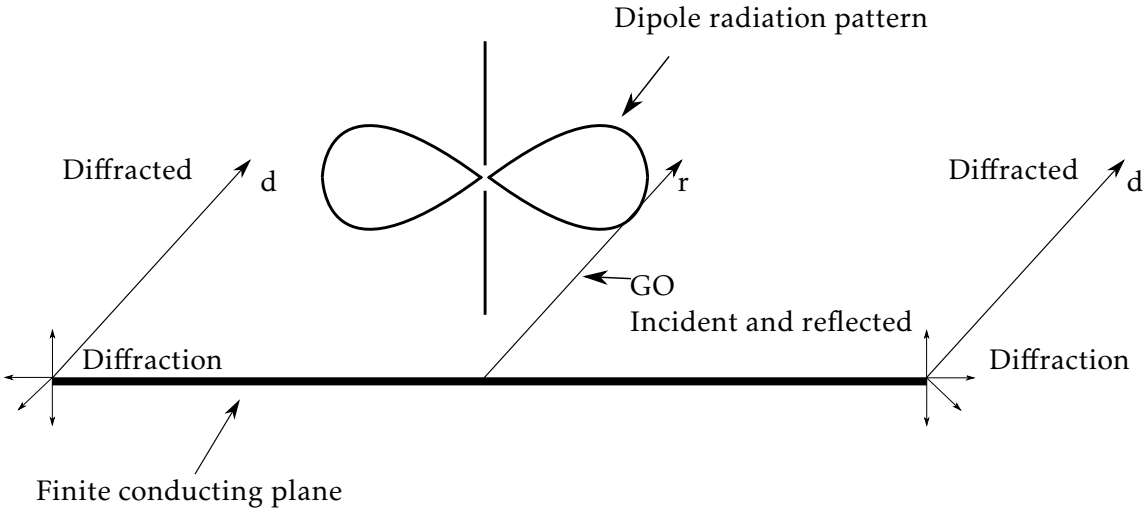

Figure 3.3: Diffraction mechanism of a dipole above a finite conductor plane [6].

As shown in Figure 3.3, there is an antenna perpendicular above the finite conducting plane and above of it. The antenna is represented as a dipole and its typical radiation pattern is shown. Therefore, it is assumed that there are waves propagating toward the conducting plane and this radiation is going to be either reflected or diffracted. In case a wave does not reach a discontinuity, a reflected ray r is produced as GO indicates. However, if a wave arrives to a discontinuity, for example the left corner of the finite conductor plane shown in Figure 3.3, many diffracted rays d are produced with the directions as a cone. Thus, the radiation pattern of a dipole is modified by many diffracted and reflected rays. These effects will be studied and shown in the analysis of the simulation results.

4 Model of an antenna on a vehicle

In this chapter, the telephone antenna which is used on the real model and the vehicle structure are introduced. Finally, a simplification of the telephone antenna and the vehicle structure is considered.

This work is focused on antenna simulations, to study the influences on the radiation pattern of an antenna when it is closed to conducting environments. With CST MWS which is a specialist tool for the 3D EM simulation of components, it is possible to obtain 3D radiation patterns and different parameters such as angular bandwidth, direction and magnitude of the main lobe or surface currents on the structure. The computation of the radiation pattern is based on the surface currents in CST MWS . The antenna under study is excited with a pulse as the transient solver is used. From the amplitude and phase of the currents, the software calculates the approximated radiation pattern due to the fact that CST MSW do not provide an exact measure. The diffraction effects are also taken into account by the currents induced on the structure next to the antenna. This radiation pattern calculation is one valid option, nevertheless there are several different theories to calculate radiation patterns. In this work, the GTD and Image Theory are considered due to the fact that they provide another vision and an easier way to understand visually the shape of the radiation pattern. Therefore, both GTD and Image theory are also two valid approximations in order to estimate the radiation pattern.

4.1 Telephone antenna

On the roof of many upper class vehicles, a roof antenna can be found. In common roof antennas several communication services as patch antennas ot telephone antennas are integrated. The focus of investigation in this work lies on the telephone antenna which has the shape of a fin and is adapted vertically to the roof. The 3D radiation pattern of the telephone antenna is shown in Figure 4.1.

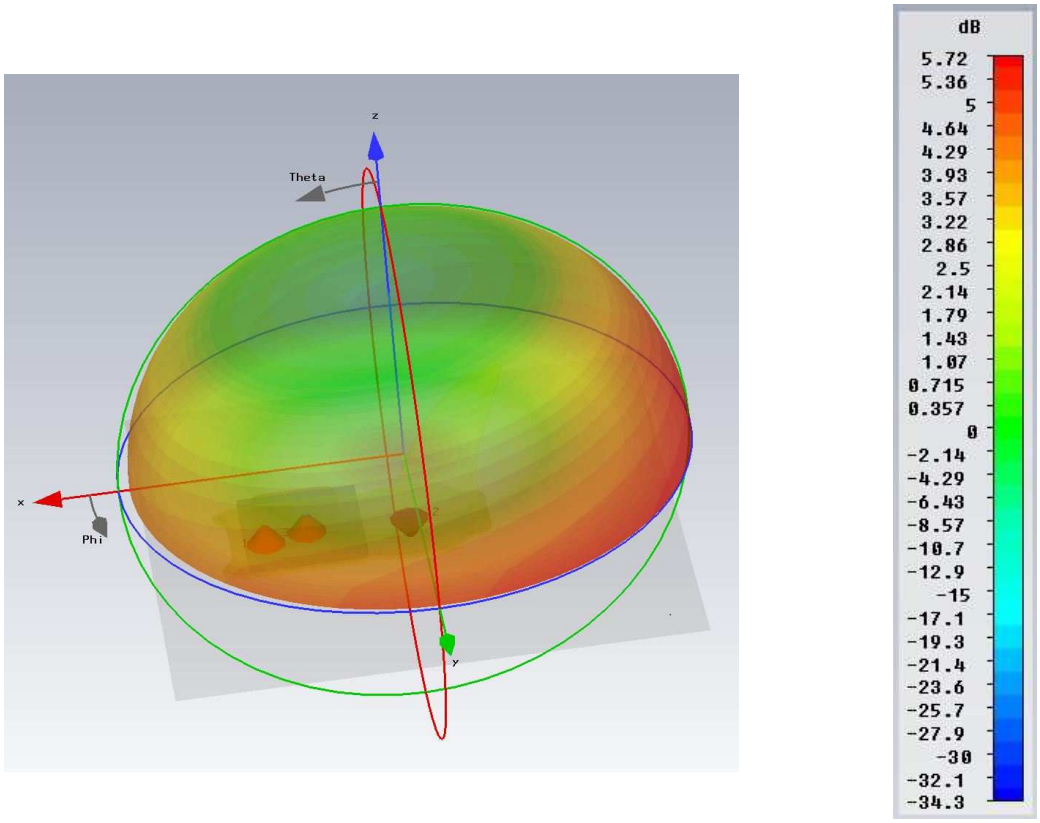

(a) Radiation pattern (b) Legend

Figure 4.1: 3D Radiation pattern of the telephone antenna. Linear polarization, θ polarized.

The radiation pattern has a radiation maximum in the direction of $-x$ axis as can be seen in Figure 4.1, but it can be approximated as nearly omnidirectional with a radiation maximum in the horizontal plane. The radiation of the telephone antenna is desirable primarily in the horizontal direction. The antenna is simulated in CST MWS with an infinite conducting wall under it to approximate the vehicle roof under it. The antenna has a high complexity so that it takes long to simulate it with CST MWS. The simulation of the telephone antenna takes nearly one day to be finished, so that the study would have not been easy to handle. The point of interest is to study the influences of conducting environments, therefore the simulation time of the antenna needs to be minimized.

Additionally, the size of the telephone antenna compared to the vehicle is very small. The vehicle has an approximate length of 4.4 m and the length of the telephone antenna is approximately 7 cm and structures on it. For this reason, the simulation of the telephone antenna with the vehicle entails problems with the CST meshing due to the fact that for the telephone

antenna is required more mesh than for the vehicle. Thus, the most restrictive part of the problem is the telephone antenna and if the mesh required for it is applied to the whole vehicle, the simulation becomes very hard to be computed. In order to reduce the time of simulation, this number of mesh cells is intended to be reduce. By reducing the number of mesh cells are reduced, the size of the mesh cells gets larger and the simulation then fails due to the fact that the size of each mesh cell is too big to take into account the antenna in the simulation.

Therefore, as the exact radiation pattern of the telephone antenna is not the most important thing to consider in this research work and due to the similarities of it to an omnidirectional antenna, a simplification is considered in the next sections.

4.2 Vehicle

Now, the vehicle model on which the antenna has to operate is introduced . The vehicle model consists basically in a real structure of a vehicle with the rear and front window. The antenna position is going to be on the back side of the vehicle roof as shown in Figure 4.2 with a red port. The structure of the vehicle is imported into CST in NASTRAN format. NASTRAN originally was a finite element analysis (FEA) program that was originally developed for NASA in the late 1960s under United States government.

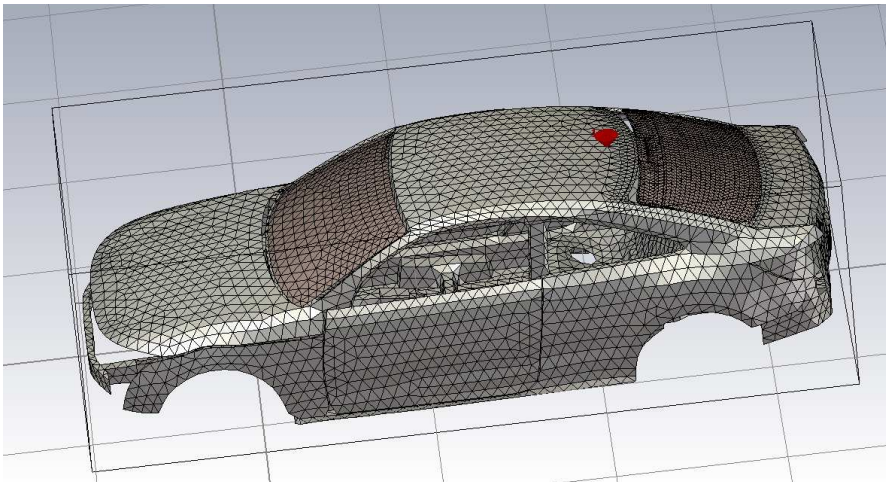

Figure 4.2: Vehicle model with windows.

To begin with the study, only the structure of the vehicle is considered, omitting the windows. The vehicle structure is made of PEC, therefore the radiation pattern is going to be influenced mainly by it. In the appendix the different views of the vehicle model are included, for example in Figure 7.1 the car views from above, below and lateral and in Figure 7.2 the front and the back side of the vehicle are shown. The maximal length of the vehicle is approximately 4.4 m and the mesh cells required in CST for simulate the whole structure are more than 100.000.000 for a five lines per wavelength and a mesh line ratio limit of three. If the mesh line ratio limit is increased more than three, the CST does not allow the meshing any more because the mesh is too dense. Moreover, the mesh line ratio limit can be decreased to

two which produces 75.000.000 mesh cells, but in this case the antenna has few lines along it. For this reason, the required time to simulate the whole vehicle takes more than one day and the viability to simulate this structure many times can not be considered. Thus, the vehicle structure also need to be simplified in order to speed up all the simulations.

The first reduction considered of the structure is shown in Figure 4.3, so that the first investigation that is done corresponds to a structure with a size around the corresponding size of the vehicle roof. The procedure to analyse the reduced structure is explained in following sections.

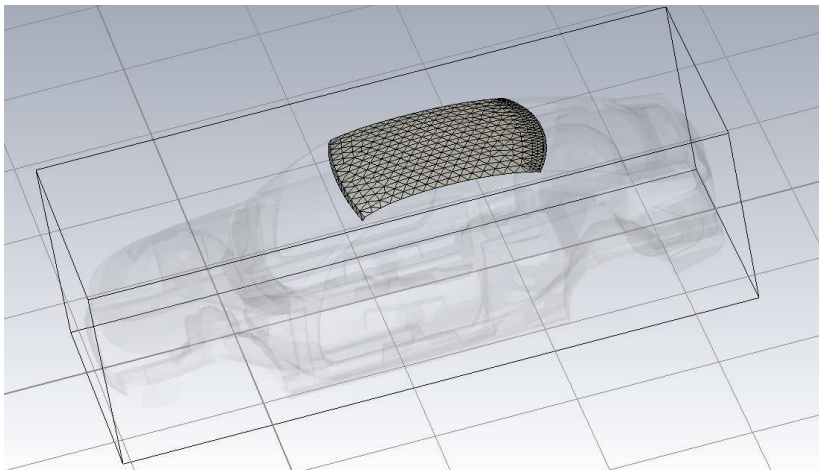

Figure 4.3: Vehicle roof.

4.3 Simplifications

In order to reduce the time that it takes to simulate the whole structure with the telephone antenna, some simplifications are considered. On the one hand, once the telephone antenna has been introduced, a simplification with it must be considered to speed up the simulations time because of the antenna complexity. If the diagram pattern of the telephone antenna is observed in Figure 4.1, and as commented before, the diagram pattern can be approximated as an omnidirectional one. Therefore, the telephone antenna seems to be replaceable by the simplest omnidirectional antenna, a dipole.

On the other hand, a reduction of the vehicle structure must be considered. For this purpose, different structure sizes are simulated to understand the effect of any possible simplification.

4.3.1 Replacement by a dipole antenna

As commented in Section 4.1, the similarities between the diagram pattern of the telephone antenna and an omnidirectional one are substantial. For this reason, a dipole is going to be the antenna under study due to the fact that with it, faster simulations are achieved and the effects of the conducting structure still can be explained independently of the antenna that is in use.

In reference to the CST solver used, there are various possible solvers to choose depending on what kind of problem is required to solve. The solver used in this work is called Time Domain Solver *T*. It is chosen because of the time domain simulation module which is capable of solving any kind of S-parameter or antenna problem. In order to simulate the structure with the *T* solver, a broadband signal is used by a port previously defined. This broadband simulation allows to obtain results such as S-parameters or radiation pattern at various frequencies. There is another solver which can be used for antenna problems which is called Frequency Domain Solver *F*. It is similar to the *T* solver due to the fact that the main task of it is the S-parameter calculations. However, the *F* solver is recommended only when small number of frequency samples need to be calculated. As an example, for lower frequency problems with a small number of mesh cells, the *F* solver could be a good alternative.

The 3D diagram pattern of a dipole with length $\lambda/2$ is shown in Figure 4.4. As can be seen, it is omnidirectional, this means that the radiation in all directions around one of the horizontal planes is equal. The corresponding dipole characteristics are shown in Table 4.1. It is optimized for a frequency of 2 GHz and its main lobe is located at 90°. It has a gain $G(\theta, \phi)$ equal to 2.16 dB and its angular width at −3 dB is equal to 75.7°.

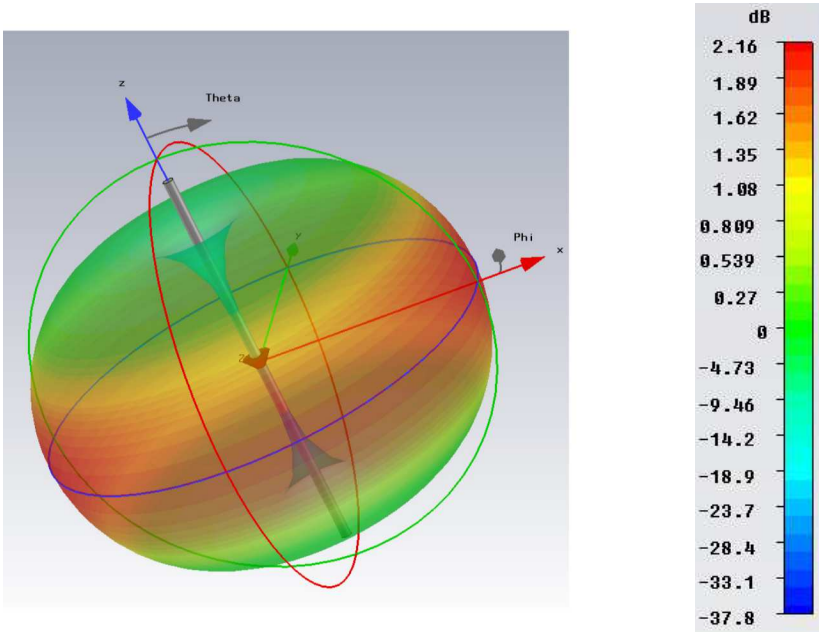

(a) Radiaton pattern (b) Legend

Figure 4.4: 3D Radiation pattern of a $\lambda/2$ dipole. Linear polarization in θ direction.

Frequency (GHz)	**Length (λ)**	**Main lobe direction (θ) / magnitude**	***Rd* (mm)**	**Angular width (-3 dB)**	**Reflection coefficient S_{11}**
2	$\lambda/2$	90°/ 2.16 dB	1.5	75.7°	-10.3 dB

Table 4.1: Dipole characteristics.

The dipole is made of PEC and is excited by a port with a impedance of 73 Ω in order to have a good impedance matching. The impedance matching is influenced by the distance, which separates the two wires which are connected by a port. The distance between the two wires is given by Kd and is approximated to a value of $\lambda/100$. In order to know whether a good impedance matching is achieved, the reflection coefficient S_{11} at the port is computed for Kd values equal to 0.06, 0.5 and 1.5 as shown in Figure 4.5. For Kd equal to 1.5, the minimum point of the S_{11} parameter is equal to −10.3 dB. This means that less than 10% of the power delivered to the antenna is reflected back into the port so that the impedance matching can be considered as good. However, the rest of simulations with different Kd values are done in order to see whether less values of Kd would provide better impedance matching as shown in Figure 4.5. Although a good approximation for Kd is chosen, in case of a value Kd equal to 0.5, better values of the minimum of S_{11} are reached, even minor than −10 dB. However, if Kd is increasingly reduced, another problem appears due to the fact that the port is too small which means that the mesh at the port is nearly one point. A Kd value equal to 0.06 is the limit from which the simulation could not be done due to the mesh. The mesh has to be more than one point in order to be able to simulate. As shown in Figure 4.5, a value Kd equal to 0.06, the minimum point of S_{11} is increased, and so there is more reflected power at the port. Thus, the approximation Kd equal to $\lambda/100$ is used from here.

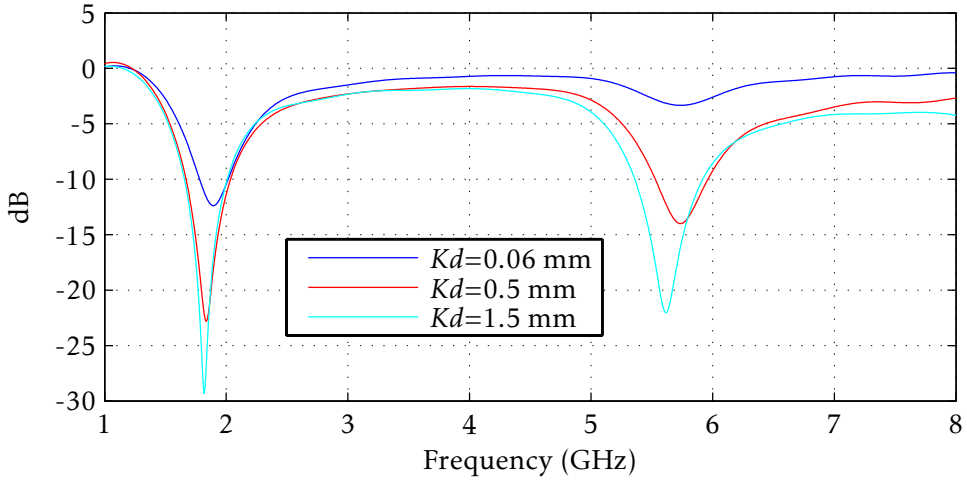

Figure 4.5: S_{11} parameter of a $\lambda/2$ dipole for Kd = 1.5 mm at 2 GHz.

The dipole is oriented along the Z axis and it has a linear polarization. In Figure 2.1 the spherical and cartesian coordinates are shown. By observing Figure 4.4, the maximum of the diagram pattern is located around the plane corresponding to $\theta = 90°$ (XY plane) and its value is 2.16 dB. The resulting radiation pattern meets the expectation from theory as can be found in [6][8]. Additionally, one analogy compare the shape of the radiation pattern could be that it is like a "Doughnut" with a hole in its middle. In Figure 4.6, different phase instants of the dipole are shown. The current on the dipole fluctuates from its maximum to its minimum between phases of 30° and 120°. As it is a $\lambda/2$ dipole, the current distribution on the it has a maximum at its middle and a minimum at its extremes [7].

The dipole length can be computed from the frequency but not the dipole thickness. The dipole thickness considered in this case is chosen with a radius *Rd* equal to 1.5 mm. Therefore, in order to prove that the dipole thickness does not affect the radiation pattern, two simulations with different dipole thickness of 2 mm and 10 mm were done. It could be observed that the radiation patterns are identical because of the surface currents which are equally distributed over the entire volume. Therefore is assumed that the dipole thickness does not affect the radiation pattern.

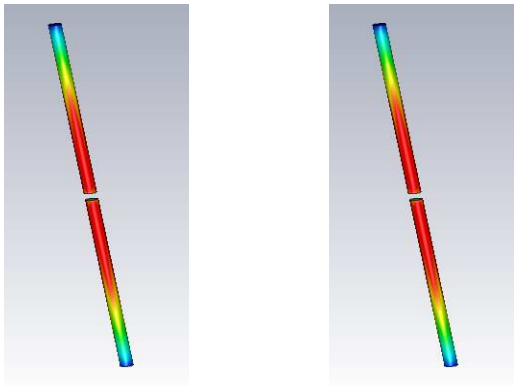

(a) Phase 30°

(b) Phase 60°

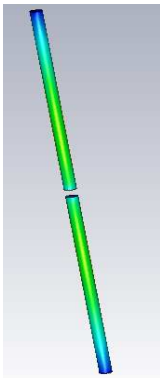

(c) Phase 90°

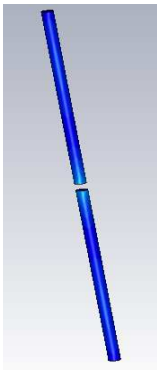

(d) Phase 120°

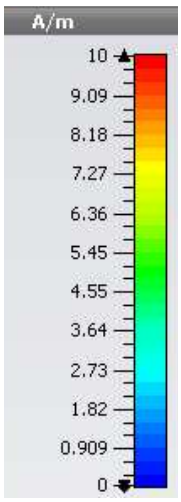

(e) Legend

Figure 4.6: Current fluctuation of a dipole for different phase instants at 2 GHz.

4.3.2 Reduction of the conducting environment

After the antenna simplification another one must be considered with the structure. The first step is to simulate a dipole perpendicular to a flat finite square plane and located above its center as shown in Figure 4.8. As commented in previous sections, a dipole is going to be considered for the study. It has a length L of $\lambda/2$, thus the plane edges are going to be considered always in reference to the dipole length. First of all, a sketch of the square plane is shown in Figure 4.7. In this kind of plane, the edge lengths Hw and Hp are equal and Tp represents the plane thickness.

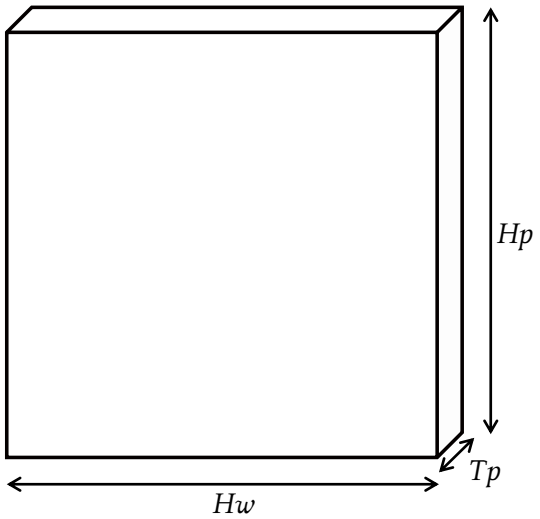

Figure 4.7: Sketch of the square plane.

In Figure 4.8, the sketch of a dipole above a conducting plane is shown. The dipole is located perpendicular to the conducting plane at a distance Kp and above its center. It has a radius represented by Rd, the distance between the two wires is represented by Kd and Hd represents the half of the dipole length . Kd is considered equal to $\lambda/100$ as commented in Section 4.3.1.

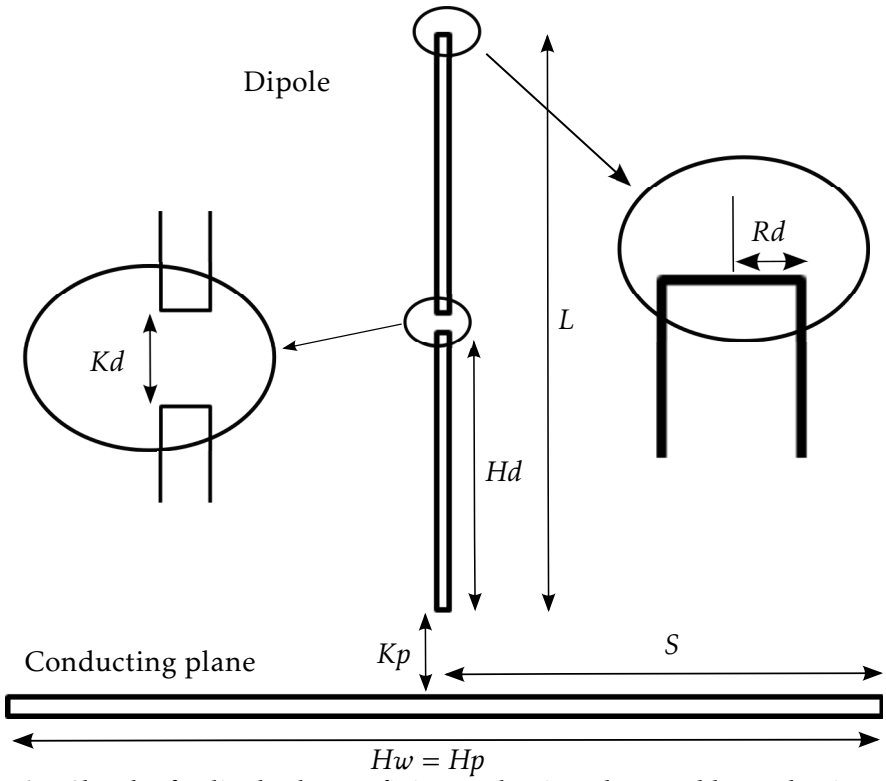

Figure 4.8: Sketch of a dipole above a finite conducting plane and located at its middle.

The first comparison is going to be among different square planes by varying its edge length Hw, Hp to investigate whether the size affects the radiation pattern and in which way. As an example, a 3D radiation pattern of the dipole perpendicular to a square plane is shown in Figure 4.9. It corresponds to an edge of the plane Hw and Hp equal to 5λ, which will be discussed later. For the first simulations, a variable S is considered to represent the half of the edge of the square plane, thus Hw is equal to $2S$, as shown in Figure 4.8. The dipole has a length L equal to $\lambda/2$, therefore the increase of S that is going to be considered each time is equal to $\frac{\lambda}{4} + \frac{\lambda}{4}i$, where i is equal to $0:7$. The results of the simulation with S equal to $\frac{\lambda}{4} + \frac{\lambda}{4}i$ for i equal to $0:3$ are shown in Figure 4.10. CST MWS provides two different gain $G(\theta, \phi)$ representations, one is Realized Gain and the other is Gain (IEEE). The Realized Gain is equal to the total gain defined in equation 2.20 but including the impedance mismatch loss. On the other hand, the Gain (IEEE) takes into account the equation 2.20 where it is related to the input or accepted power of the structure without the impedance mismatch loss consideration. In this work, the Gain (IEEE) representation is used.

As can be observed in Figure 4.10, when S is equal to the half of the dipole length S equal to $\lambda/4$, represented by blue colour, the size of the plane is such small that there is very little influence on the radiation pattern when comparing to the dipole simulation represented by red colour. The dipole simulation characteristics are shown in Table 4.1. However, the following increase of S, represented by pink colour, shows that symmetrical side lobes approximately at θ equal to 155° appear. The simulation corresponding to S equal to $3\lambda/4$ and represented

by black colour, shows that symmetrical side lobes on the upper part of the radiation pattern starts to appear and the lower side lobes remains. When a value of S equal to an integer multiple value of L is reached, as it is the case with S equal to $2L$, those upper side lobes are stronger and two more at the lower part of the radiation pattern rise up. It seems that when S is equal to an integer multiple value of the dipole length, this fact produces the apparition of symmetrical side lobes in the lower part of the radiation pattern and the upper side lobes become more sharper.

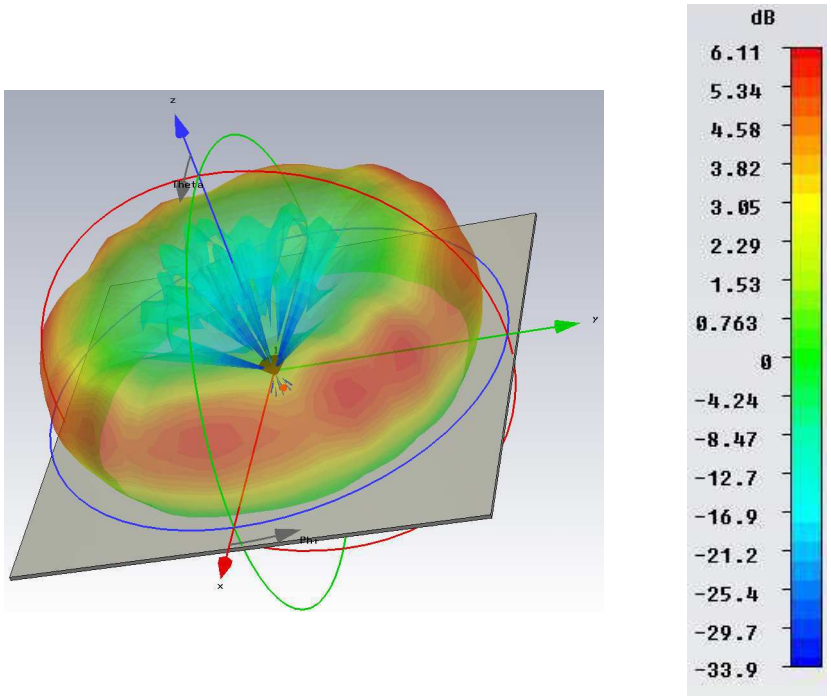

(a) Radiation pattern (b) Legend

Figure 4.9: 3D Radiation pattern of a dipole perpendicular to a square conducting plane. Linear polarization in θ direction.

The results of the simulation with S equal to $\frac{\lambda}{4} + \frac{\lambda}{4}i$ for i equal to $3:7$ is shown in Figure 4.11. The simulation corresponding to a S equal to $2L$, represented by red colour, is the same simulation represented by green colour in Figure 4.10. It is shown again to see the progression of the radiation pattern shape until a S equal to $4L$. Now, by observing the simulation represented by pink colour, new symmetrical lower lobes appear. A certain relation between L, S and the side lobes remains. In fact, if the result of the simulation with S equal to $2L$ represented by red colour is observed, four lower and two upper side lobes appear. Afterwards, in case of a S equal to $3L$, two symmetric side lobes are added to the upper and lower part of the radiation pattern, so that in the end, it has six lower and four upper side lobes. Finally, in case of the simulation with S equal to $4L$, the same effect occurs and two more symmetric side lobes are added again. In this last case, there are eight lower and six upper side lobes.

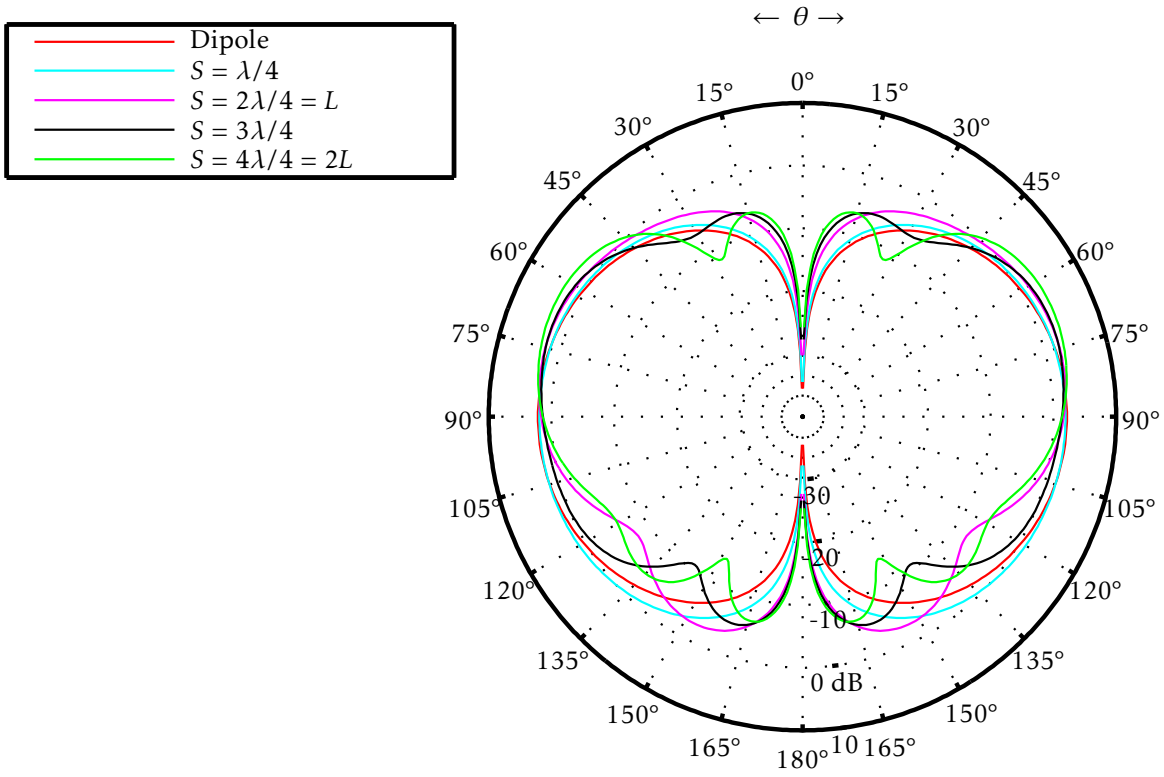

Figure 4.10: Gain in dB of a dipole perpendicular to square planes of different S values, (θ, $\phi = 90°$).

As a consequence, a rule can be established in case of a dipole of length L equal to $\lambda/2$ with a distance Kp equal to 3.4 mm from the plane. According to the simulation results, a clear dependency among L, S and the number of lower side lobes exists. The main lobe also depends on S and as it is increased the main lobe becomes narrower. If the edge length of the plane is chosen to be an integer value of L, the number of lower side lobes that will appear are going to be equal to the edge length of the plane over the length of the dipole as shown in equation 4.1.

$$\text{n° of lower side lobes} = \frac{Hw}{L} = \frac{Hp}{L} = \frac{2S}{L} \tag{4.1}$$

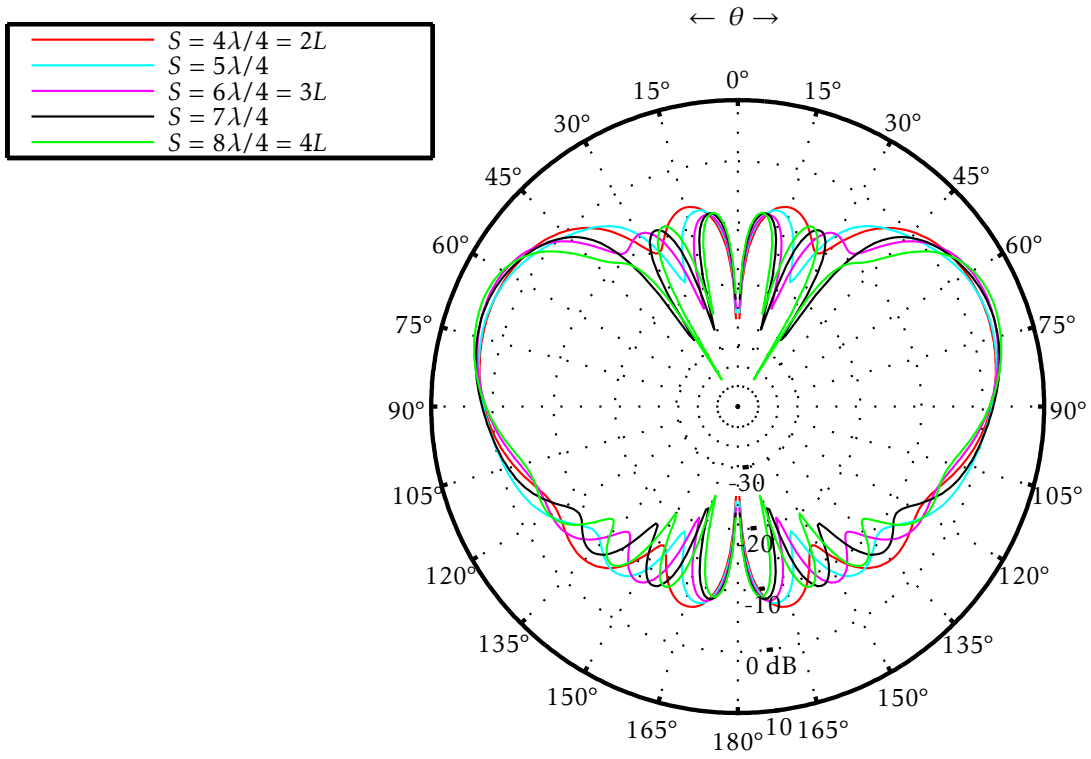

Figure 4.11: Gain in dB of a dipole perpendicular to square planes of different S values, (θ, $\phi = 90°$).

After the clear dependency of the radiation pattern with the edge lengths of the plane , which are always in relation to the dipole length, more simulations are done to show until which plane size the effects on the radiation pattern need to be considered. For this, another comparison amongst different edge lengths of the square plane is done and shown in Figure 4.12. The characteristics of these simulated structures are shown in Table 4.2. Furthermore, the corresponding characteristics for each simulation are shown in Table 4.3. The spherical coordinate system used to represent the results is shown in Figure 2.1. The simulation results are represented as the angle of θ in degrees vs gain $G(\theta, \phi)$ in dB.

Hw = Hp	***f*(GHz)**	**λ(mm)**	***Rd***	***Hd***	***Kd***	***Tp***	**Material**	***Kp***
1λ	2	150	1.5	37.5	1.5	6.4	PEC	3.4
5λ	2	150	1.5	37.5	1.5	6.4	PEC	3.4
10λ	2	150	1.5	37.5	1.5	6.4	PEC	3.4
20λ	2	150	1.5	37.5	1.5	6.4	PEC	3.4
50λ	2	150	1.5	37.5	1.5	6.4	PEC	3.4

Table 4.2: Characteristic of the dipole and square plane.

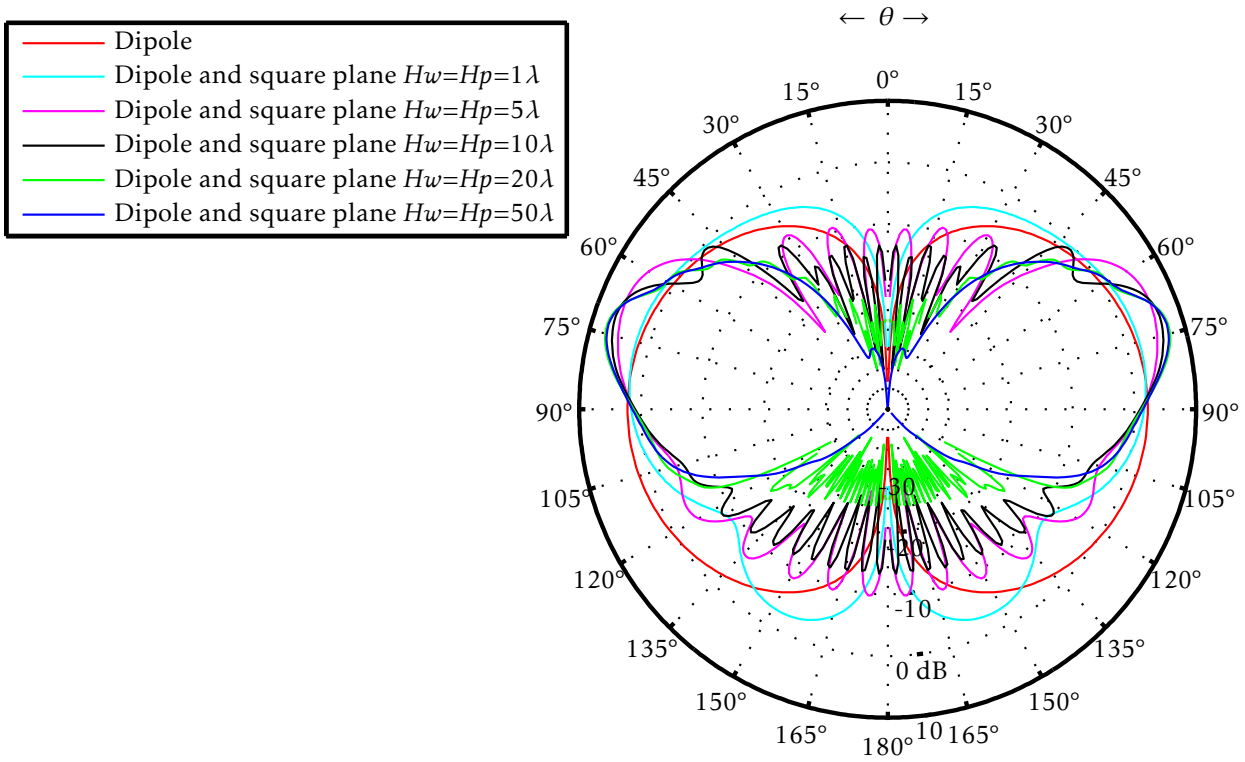

Figure 4.12: Gain in dB of a dipole perpendicular to square planes of different sizes (θ, $\phi = 90°$).

Hw = Hp	**Main lobe direction (θ)**	**Main lobe magnitude**	**Angular width (-3dB)**	**Reflection coefficient S_{11}**
1λ	77°	2.2 dB	57.7°	-7.74 dB
5λ	68°	5.9 dB	28.5°	-7.13 dB
10λ	71°	6.6 dB	21°	-6.64 dB
20λ	73°	7.5 dB	17.3°	-7.12 dB
50λ	73°	7.2 dB	17.7°	-7.35 dB

Table 4.3: Characteristics of the simulation shown in Figure 4.12.

At first glance in Figure 4.12, the radiation pattern corresponding to an edge length of Hd and Hw equal to 20λ and represented by green colour, is practically equal to the edge length of Hd and Hw equal to 50λ represented by dark blue. It seems that after an edge length of 50λ, there are many very small side lobes that are not visible and can be ignored. There are also only slight differences between both simulations, the shape of the main lobes are practically equal and only the side lobes differ from each other. Therefore, it seems that a

possible threshold for the structure reduction could be an edge length of Hd and Hw equal to 20λ. Thus, the current distribution induced on the conducting plane is investigated. In Figure 4.13, the current distribution of some simulations is shown. In Figure 4.13 (a), the maximum current magnitude is over almost all the plane surface flowing to each corner and edge. However, as the edge length of the plane is increased, the current magnitude decreases at the discontinuities. In Figure 4.13 (d), the measured current at the corners and edges is minor than the 0.25% of the maximum current magnitude in the dipole.

Hence, if the edge length of the plane is increased to more than 20λ, the effects of a further increase of edge length on the radiation pattern are minimal. In fact, as shown in Table 4.3, the main lobe resulting of the simulation with edge length 20λ is more directive than the main lobe of the 50λ one. The radiation pattern shape between both are quite the same, only side lobes appears in the radiation pattern corresponding to an edge length of Hd and Hw equal to 20λ. Nevertheless, as shown in Figure 4.12, these side lobes have a gain around $-25dB$ and their influence could be ignored.

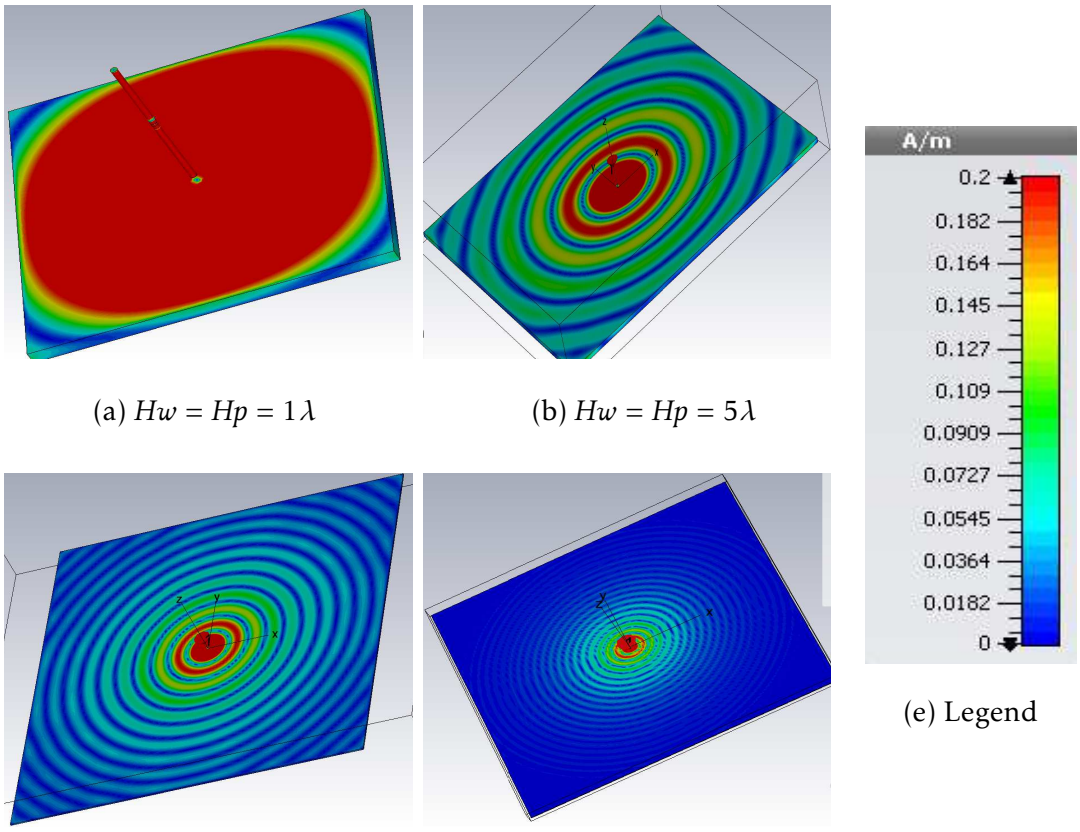

(a) $Hw = Hp = 1\lambda$ (b) $Hw = Hp = 5\lambda$

(c) $Hw = Hp = 10\lambda$ (d) $Hw = Hp = 20\lambda$

(e) Legend

Figure 4.13: Surface currents corresponding to the different edge lengths of the square conducting plane.

As a consequence, a possible structure reduction based on the results of the current distri-

bution and the far field radiation patterns can be considered. A finite conducting plane of edges Hd and Hw equal to 20λ could be assumed as a good compromise for the reduction.

Finally, the effect on the radiation pattern due to the structure material is studied. For this, three simulations with different material types are done. In Figure 7.3, the comparison among the structure under study made of different materials is shown. The lossy metal materials used are aluminium and copper and their dielectric constants are 2.2 and 2.8 respectively. The results showed that the radiation pattern was equal independently of the material used. Hence, PEC material is going to be considered from here for all the simulations.

5 Influences on the antenna behaviour

After the decisions about necessary reduction of the structure and the antenna were made, the idea is to make a study about how the radiation pattern changes when it interacts with its surrounding, in this case conducting environments. The procedure is to simulate different structures close to the antenna and investigate how the radiation pattern with different structure shapes, edge lengths and other characteristics changes.

First of all, several structure attributes are investigated, as for example the plane shapes in order to see if the shape has an influence on the radiation pattern or for example the structure curvature. In order to explain the effects on the radiation pattern, two theories introduced in previous chapters are used. Thus, in Chapter 5.2, the Image theory is verified and the effects of GTD are investigated.

Finally, the whole vehicle is studied and the effects are explained based on the previous results.

5.1 Attributes of the simplified model

The aim of this section is to investigate the influence of different attributes of the conducting plane. For this purpose, the effect of corners and edges of a finite plane or the effect of a curved plane are studied in order to explain the radiation pattern of an antenna on the vehicle roof.

5.1.1 Corners and edges

Conducting environments can become very complex. In case of vehicle structures, they are usually made with quite thin thick sheet metal. Thus, the first step is to simulate different shapes of conducting planes in order to see the different effects on the radiation pattern.

The first type of finite plane under study has been introduced in Section 4.3. It is a square plane made of PEC, where a dipole is located perpendicular to the plane and above its center, as shown in Figure 4.9. The characteristics concerning to the square planes as well as the simulation results were shown in Section 4.3. The radiation pattern of the dipole without surrounding is represented by red colour and its characteristics are shown in Table 4.1. It is shaped by two lobes which are the main lobes of the radiation pattern and their radiation pattern maximum is located at $\theta = 90°$. The gaps that can be seen at $\theta = 0°$ and $180°$ are due to the dipole position, therefore there is never radiation in the directions where the dipole is.

The simulation represented by blue colour, belongs to the radiation pattern of a dipole perpendicular to a conducting plane of edge lengths Hd and Hw equal to 1λ. As seen in Section

4.3, whether the plane edge length is increased with a value equal to the dipole length L, symmetric side lobes appear on the radiation pattern. As shown in Figure 4.12 and according to the equation 4.1, the number of lower side lobes are two. In addition, if the previous simulation is compared with the blue one, when the square plane is present, the main lobe becomes narrowed and more directive. The angular width at -3 dB also changes from 75.7° in the dipole case to 57.7° in the dipole with square plane case. Moreover, in the blue simulation, the radiation maximum is located at 77° instead of 90° as occurs in case of the red one. The plane seems to affect the inclination of the radiation pattern tending to enhance it upwards, besides the angular width at -3 dB gets narrowed and the directivity is increased.

In fact, as the edge length of the plane is increased, the effect becomes clearer. The simulation represented by pink colour, belongs to the radiation pattern of a dipole perpendicular to a conducting plane with edge lengths Hd and Hw equal to 5λ. In this case, the effect of the conducting plane enhances more the inclination of the radiation pattern maximum. Comparing the blue simulation to this one, the angle of the radiation pattern maximum changes from 77° to 68° and its gain maximum from 2.2 dB to 5.9 dB as shown in Table 4.3. Furthermore, the main lobe becomes narrower with an angular width at -3 dB of 28.5° and according to the equation 4.1, the number of lower side lobes that appear are ten. A trend is also observed with respect to the side lobes. As the edge length is increased, there is a plane effect which seems to cancel the radiation under it. Comparing the previous simulation to this one, the side lobes become weaker. If the edge length is increased to Hd and Hw equal to 10λ, corresponding to the simulation represented by black colour, the inclination of the main lobe is now decreased. It seems that as the plane edge length is increased, the inclination tends to converge to an angle around 73° besides in this case the number of side lobes according to the equation 4.1 are twenty. However, the cancellation effect becomes clearer due to the fact that the side lobes are getting weaker and the gain maximum is increased to 6.6 dB. Thus, there are three trends which can be distinguished. The first one is the inclination of the main lobe due to the reflections of the conducting plane. The second one is the antenna directivity, which as the plane edge length is larger, the antenna becomes more directive. And the last one is the cancellation of the radiation downward the conducting plane.

Finally, the two last simulations represented by green and dark blue colour, belong to the simulations with edge lengths of Hd and Hw equal to 20λ and Hd and Hw equal to 50λ respectively. Following the three trends commented above is observed that the inclination of the main lobe for both cases is slightly increased. The maximum of the radiation pattern among all the simulations commented, fluctuates between the angle of θ equal to 68° and 77° to finally converge at 73°. This means that the conducting plane affect the radiation pattern inclination but this inclination is not increased gradually according to the edge length. With a small plane size it jumps to a high value but when the size is bigger the angle converges to θ equal to 73°. On the other hand, the main lobe still becomes narrower and more directive. In case of the green simulation, the main lobe magnitude is 7.5 dB and in case of the black one it is 7.2 dB, which is slightly less. The radiation pattern in both simulations is very similar, only the side lobes differentiate them, therefore this can be the reason why the main lobe magnitude is slightly reduced in the dark blue simulation. The most clear trend is the cancellation effect of the plane. As can be seen in the green simulation, the side lobes are reduced until a gain $G(\theta, \phi)$ around -30 dB so that they can be ignored. Considering this

reduction, the simulation represented in green and dark blue can be approximate as equal and the simulation corresponding to a edge length of Hd and Hw equal to 20λ is considered a good approximation.

Thus far, a square shape as plane has been studied. Now, is interesting to study how the radiation pattern changes among different plane shapes to see whether the trends are produced in a different way if there are no corners, so a circular plane is considered. As an example, in Figure 5.1 the 3D radiation pattern of a circular plane corresponding to a radius of Rp equal to 2.5λ is shown. The main lobe shape in case of the circular plane is curved due to the rim of the plane. The side lobes are more intense than in case of the square plane. The sketch of the dipole and the plane is shown in Figure 4.8. The particular sketch of the circular plane and its characteristics are shown in Figure 5.2 and Table 5.1 respectively.

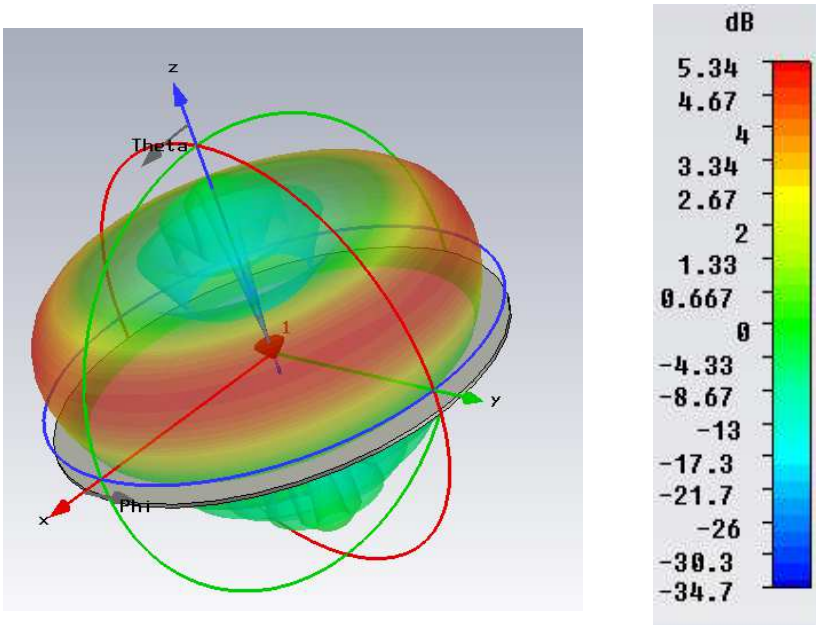

(a) Radiation pattern (b) Legend

Figure 5.1: 3D Radiation pattern of a dipole perpendicular to a circular conducting plane. Linear polarization in θ direction.

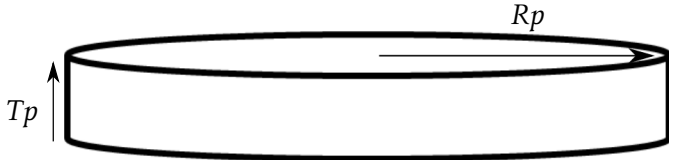

Figure 5.2: Sketch of the circular plane.

Rp	*f*(GHz)	λ(mm)	*Rd*	*Hd*	*Kd*	*Tp*	Material	*Kp*
0.5λ	2	150	1.5	37.5	1.5	6.4	PEC	3.4
2.5λ	2	150	1.5	37.5	1.5	6.4	PEC	3.4
5λ	2	150	1.5	37.5	1.5	6.4	PEC	3.4
10λ	2	150	1.5	37.5	1.5	6.4	PEC	3.4

Table 5.1: Characteristics of the dipole and circular plane structure.

The simulation characteristics corresponding to each one are shown in Table 5.2 and the result of the comparison among the dipole perpendicular to different sizes of the circular planes is shown in Figure 5.3.

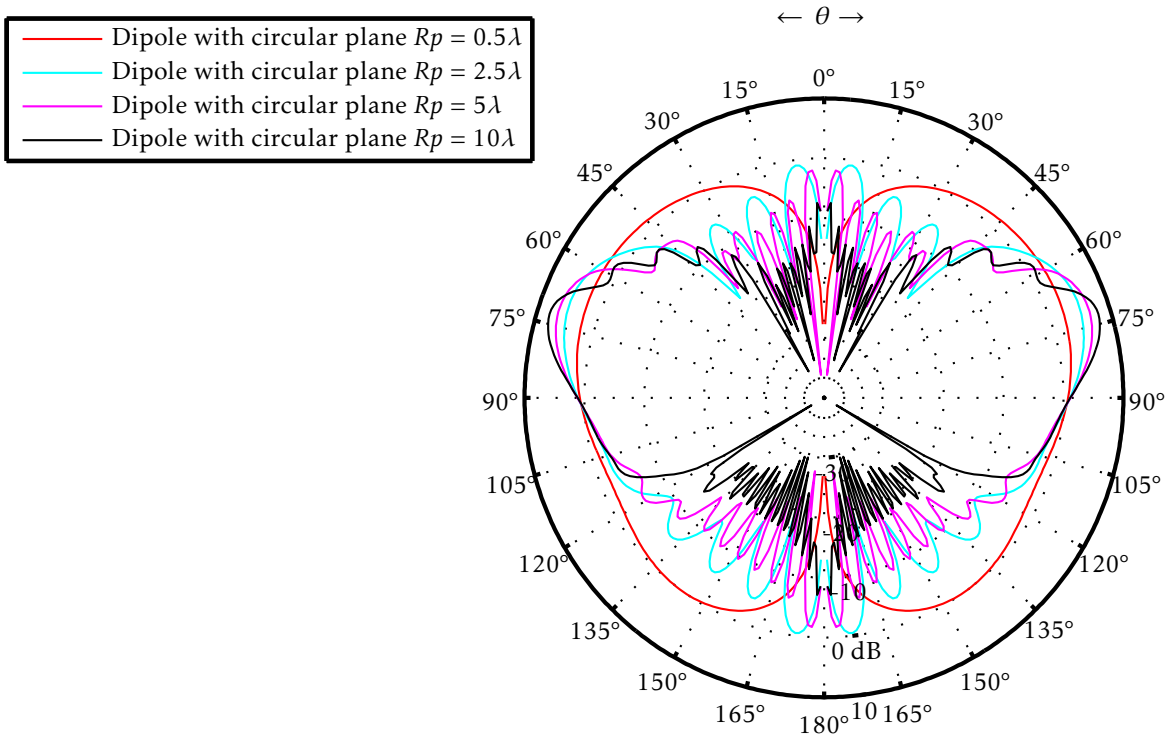

Figure 5.3: Gain in dB of a dipole perpendicular to circular planes of different sizes (θ, ϕ = 90 °).

Rp	**Main lobe direction (θ)**	**Main lobe magnitude**	**Angular width (-3dB)**	**Reflection coefficient S_{11}**
0.5λ	69°	5.3 dB	30°	-6.6 dB
2.5λ	69°	5.3 dB	30°	-6.6 dB
5λ	71°	6.6 dB	23°	-7 dB
10λ	73°	7.9 dB	16°	-7 dB

Table 5.2: Characteristics of the simulations shown in Figure 5.3.

As the effect of the edges and corners is much small with a square plane size of 50λ or more, the size is reduced to 20λ now. This square size corresponds to a circular plane radius Rp equal to 10λ. For the circular conducting plane four simulations were made. At first glance, the radiation pattern symmetry in Figure 5.3, seems to be horizontal and vertical for short plane radius like Rp equal to 2.5λ and 5λ. Moreover, equation 4.1 for this case remains valid, so the number of lower side lobes depend on the plane radius in integer number of dipole lengths. Following the same trends as before, in case of the circular plane the inclination of the main lobe behaves in the same way as the square plane. For short edge lengths, like Rp equal to 0.5λ or 2.5λ, the inclination is greater but when the edge length is increased more, the inclination gets smaller until an angle of 73°. Regarding to the directivity, it increases as well as the edge length is increased reaching higher gain magnitudes. The plane cancellation effect is also visible, so that when the plane becomes larger the radiation under it has lower gain magnitude. In general, the differences between a square plane and a circular plane are that for a circular plane, the side lobes near the axis corresponding to θ equal to 0° and 180° are more intense than for the square plane. Respect to the rest of trends, they remain very similar.

The presence of a finite conducting plane in principle can be analysed with image theory as explained in Section 3.1. It can be taken into account if an infinite perfect conducting plane is considered. Having an infinite plane is not realistic, nevertheless in case of large finite planes, the image theory can be applied as well. Considering the results of the finite square plane in Subsection 4.3.2, it can be seen that after an edge length of Hw and Hp equal to 20λ the plane could be approximated as an infinite one. The variations of the radiation pattern between a square plane of edge Hw and Hp equal to 20λ and Hw and Hp equal to 50λ can be neglected, due to the fact that the main lobes are approximately equal and the side lobes in the Hw and Hp equal to 20λ case can be obviated because of the low gain magnitude. Thus, the radiation pattern shape can be analysed as the contribution of the direct wave and all the reflections due to the finite conducting plane [6]. If the reflections are taken into account, the conducting plane can be substituted as a symmetric virtual dipole at a distance of $2h$ from the real one as shown in Figure 3.1. This case is going to be verified in Section 5.2. Hence, the radiation pattern of the dipole above the conducting plane is in part formed by the radiation pattern of the real dipole and the contribution of a virtual dipole emanating the same radiation as the

real dipole toward it. Therefore, the reflections on the conducting plane can be approximated to the radiation of the virtual dipole.

Taking into account not only the fact of having a conducting plane under the antenna. If a conducting plane is finite, this limitation entails the existence of corners and edges. If a wave arrives to a discontinuity, geometrical optics is no longer valid because of the reflections on the extremes that cannot be considered as a normal reflection on the surface. For that reason another effect has to be taken into account, the interaction of a wave with an edge or corner implicates many diffracted rays which can be explained by the Geometrical Theory of Diffraction (GTD)[7][21]. The resulting radiation pattern shape is not only due to the presence of a very large conducting plane but also the fact that it has discontinuities which are going to produce more diffracted rays. Therefore, in case of the square plane, the radiation pattern shape is affected by the effect of the reflections on the finite plane and the diffracted rays due to the edges and corners.

According to the simulation results in Figure 4.12, comparing the simulations of Hw and Hp equal to 20λ and Hw and Hp equal to 50λ, the diffraction effect in case of $Hw = Hp = 50\lambda$ is no longer influencing considerably to the radiation pattern. The radiation patterns are approximately equal. Thus, there is a relation between the size of the plane and the effect of the diffraction. There is a threshold from which, the radiation diagram remains nearly equal due to the low intensity of the radiated waves at the discontinuities. Regarding the circular plane, there is a difference in respect to the square one. When the diffraction is produced by curved edges instead of straight ones, they create caustic. A caustic is a point or a line through which all the rays of a wave pass, as for example the focal point of a paraboloid [7]. Mathematical methods of scattering calculation and GTD are developed in [6][7][19] and [22]. As in Figure 4.12 and 5.3, one simulation for a square plane and one for a circular plane are done in [6] and [7]. There were shown the same trends and similar results for a dipole with length of $\lambda/4$. The $\lambda/4$ dipole shows a difference between considering only GO and considering GO and GTD together. In addition, when a finite plane is considered, there is not only diffraction because of the edges. There is also diffraction between edges due to the finite plane thickness and size. For this reason, there are more diffractions due to the diffracted rays among corners. The diffraction mechanism between corners of a finite plane is shown in Figure 5.4.

In this case, after the wave is diffracted, one of the resulting diffracted rays propagates from point 1 to point 2. This means that when the diffracted ray arrives to the point 2, it is diffracted again in all directions including a ray towards the point 1 again. This re-diffracted rays are called *higher-order diffractions* and they result in coupling between edges [7]. Figure 5.4 is an example of the diffraction mechanism at only one point of the edge, in this case the corner, but this mechanism is applicable to any point of the edge. This means that not only the first diffracted ray of the edges are corners is contributing to the radiation patter but in each point, each re-diffracted ray affects the radiation pattern. So, n rays will be re-diffracted several times contributing to the dipole radiation pattern until the ray is weak enough so that the influence of the next re-diffracted rays to the radiation pattern can be ignored. In case of having a very large edge, the rays that contribute to the radiation will be less intensive. Therefore the radiation pattern will keep nearly the same shape independent from the edge length which is further increased.

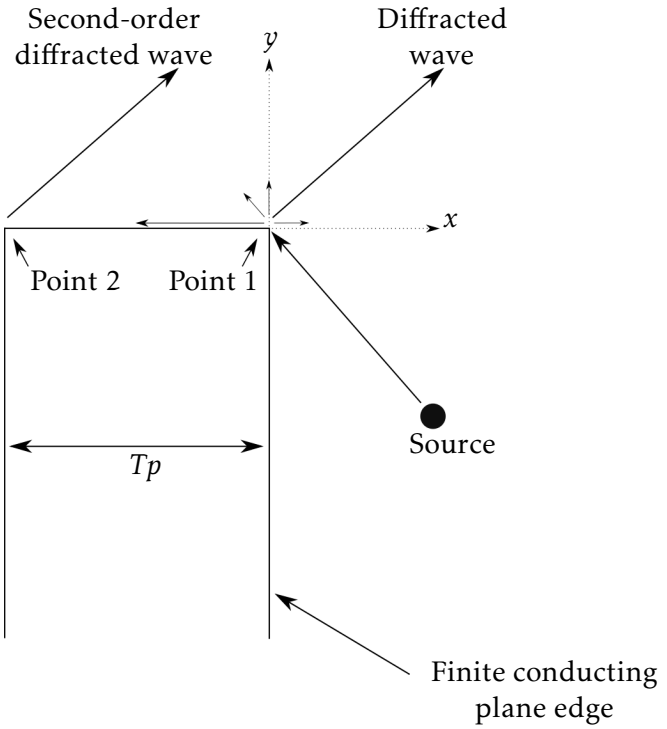

Figure 5.4: Diffraction mechanism for an edge of finite thickness [7].

Reviewing the study until here, the effects due to the reflections and due to the diffractions are mostly on the side lobes and the fact that the lobes shape are not perfectly curved but they have some kind of ripple. There is also the radiation cancellation due to the conducting plane but this effect seems to be more clear when the plane is larger. This is because, as the diffraction effects become weaker, the reflected waves on the plane surface reinforce the radiation cancellation. In addition, the effects due to the reflections and the diffractions are studied in more detail in Section 5.2. As support to the circular plane results, a comparison among the surface current on the different radius lengths are shown in Figure 7.4. The radius length of Rp equal to 10λ corresponding to a square edge length of Hw and Hp equal to 20λ remains the optimal with less than 0.25% of the dipole current maximum at the discontinuities of the plane. Same trend as the square plane in Subsection 4.3.2.

Finally, in order to investigate the influence of having different shapes of the finite conducting plane, two more plane shapes are simulated and compared with the square and circular one. These plane shapes are with cut corners similar to an octagonal plane and with bended corners. They follow the same sketch and the characteristics as shown in Figure 4.8 and Table 4.2. A 3D radiation pattern for the octagonal and bended plane and their structure are shown as an example in Figure 7.5 and 7.6 respectively. The comparative among the four different plane shapes for Hw and Hp equal to 5λ, Rp equal to 2.5λ and its characteristics are shown in Figure 5.5 and Table 5.3 respectively.

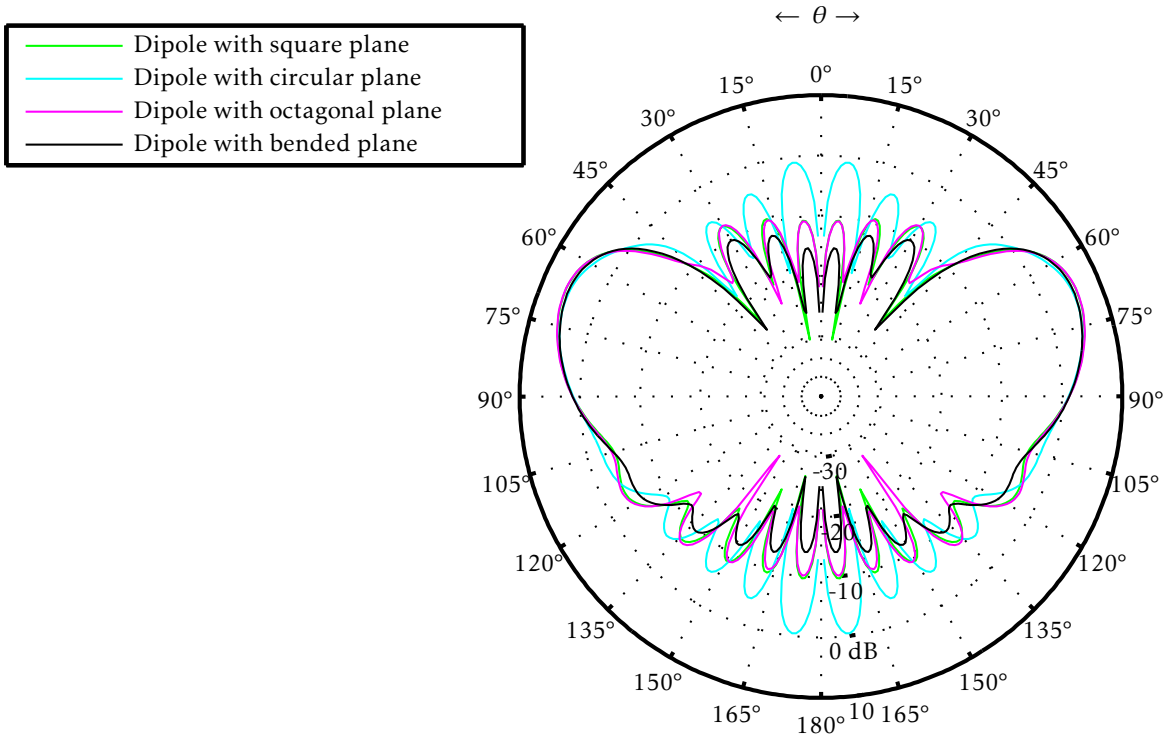

Figure 5.5: Gain in dB of a dipole perpendicular to a square, circular, octagonal and bended plane (θ, $\phi = 90°$) for $Hw = Hp = 5\lambda$ and $Rp = 2.5\lambda$.

Plane shape	**Main lobe direction (θ)**	**Main lobe magnitude**	**Angular width (-3dB)**	**Reflection coefficient S_{11}**
Square	68°	5.9 dB	28.5°	-7.1 dB
Circular	69°	5.3 dB	30°	-6.6 dB
Octagonal	68°	5.9 dB	28.2°	-7.1 dB
Bended	68°	5.4 dB	30.4°	-7.2 dB

Table 5.3: Characteristics of the simulations shown in Figure 5.5.

As can be observed in Figure 5.5, the square plane simulation represented by green colour and the octagonal plane simulation represented by pink colour are very similar. The octagonal plane is just the square plane with the corners cut, therefore in this case there are four large edges, four shorter edges and eight corners. It seems again that the diffraction affects in more proportion according to the edge length instead of the number of corners. At any rate, the differences between them are quite a few, only the curved edges, for example circular or bended edges makes a big difference when the edge length is short, for example the edge

length Hw and Hp equal to 5λ considered in Figure 5.5.

The simulation represented by black colour belongs to the bended plane and the simulation represented by blue colour belongs to the circular plane. The circular plane simulation, shows again the differences of the side lobes which are more intensive due to the caustics that create the curved edges. However, the bended plane is a mixture of square and circular shapes, and it makes the side lobes less intensive than the circular plane for edge length of Hw and Hp equal to 5λ. In this way, the simulation results show that for short edge length, case in which the plane is not approximate to the infinite one, the diffraction effects are strong.

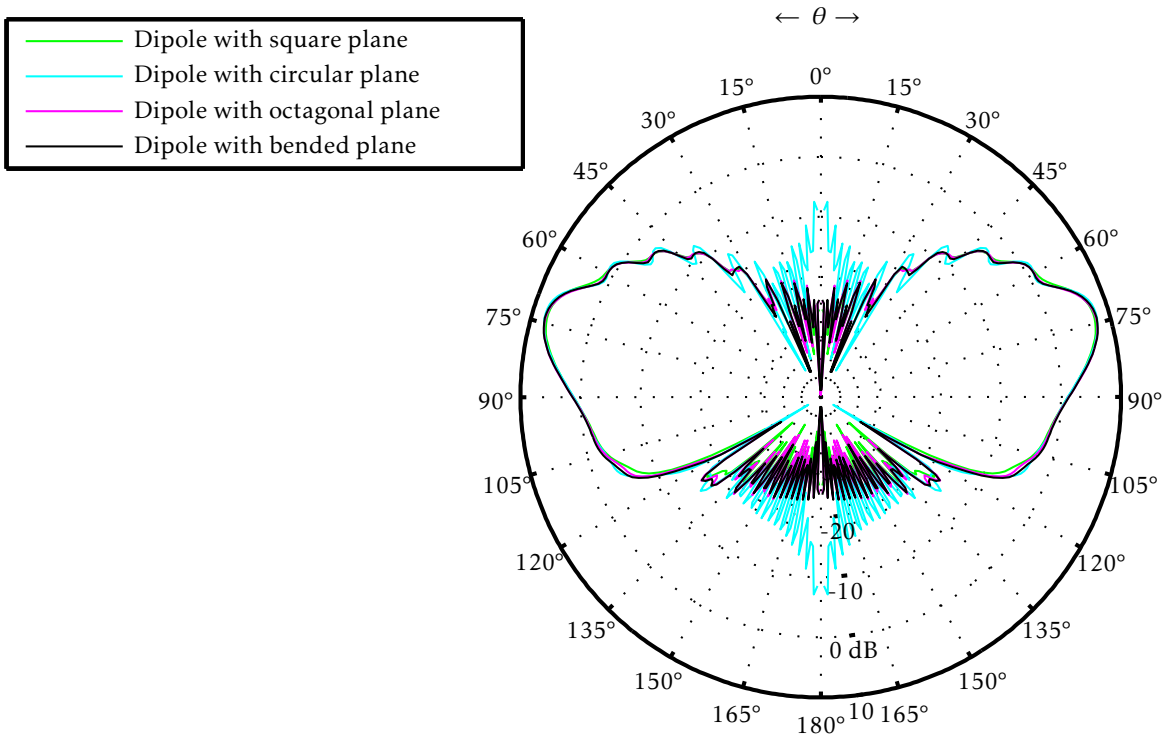

Figure 5.6: Gain in dB of a dipole perpendicular to a square, circular, octagonal and bended plane (θ, $\phi = 90°$), for $Hw = Hp = 20\lambda$ and $Rp = 10\lambda$.

Considering the trends until here, if an edge length of Hw and Hp equal to 20λ is considered so that the plane can be approximated to an infinite one, the differences among different plane shapes are minimum. For this purpose, the comparative among the four different shapes of the plane corresponding to Hw and Hp equal to 20λ and Rp equal to 10λ is shown in Figure 5.6. The characteristics of each simulation is shown in Table 5.4. In this case, the three simulations corresponding to the square, bended and octagonal plane are nearly equal, only the circular plane makes again a slight difference. Therefore an edge length of Hw and Hp equal to 20λ shows that is a good threshold form which the diffraction has minimal effect.

Plane shape	Main lobe direction (θ)	Main lobe magnitude	Angular width (-3dB)	Reflection coefficient S_{11}
Square	73°	7.5 dB	17.3°	-7.1 dB
Circular	73°	7.9 dB	16°	-7 dB
Octagonal	74°	7.7 dB	16.8°	-7.1 dB
Bended	74°	7.8 dB	16.6°	-7.1 dB

Table 5.4: Characteristics of the simulations shown in Figure 5.6.

In conclusion, if Figure 5.4 is observed, can be assumed that when the size of the plane is equal or greater than the threshold Hw and Hp equal to 20λ, the plane shape does not make a difference. Only a curved edge differ because of the caustics. These caustics or points through which the rays pass, concentrate concentrated the energy what means more intense side lobes. Therefore the caustics reinforce the radiation from θ equal to 0° to nearly 30° besides the area corresponding to the symmetric angles.

5.1.2 Curvature

Thus far, only flat finite conducting planes have been considered. However, the vehicles are made from curved structures as for example the vehicle roof. Therefore, in the following subsection, curved structures are investigated in order to see whether the curvature of a conducting plane has considerable influences in the diagram pattern.

For this purpose, the curvature effect is investigate before the study of the vehicle roof. But first of all, the details of the vehicle roof are explained. In Figure 5.7, a sketch of the vehicle roof is shown. Its dimensions are Hw around about 10λ and Hp around about 7λ and as can be seen its edges are rather curved instead of straight. Thus, it is comparable to a plane edge of Hw equalt to 10λ or a radius of Rp equal to 5λ. So, due to the fact that the edges are not straight, it is considered comparable to a circular plane. The 3D radiation pattern of the vehicle roof and its characteristics are shown in Figure 5.8 and in Table 5.5 respectively.

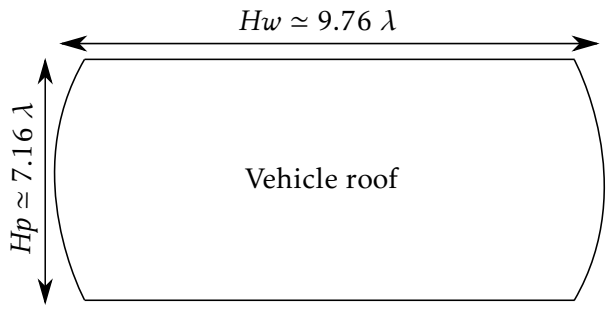

Figure 5.7: Sketch of the vehicle roof.

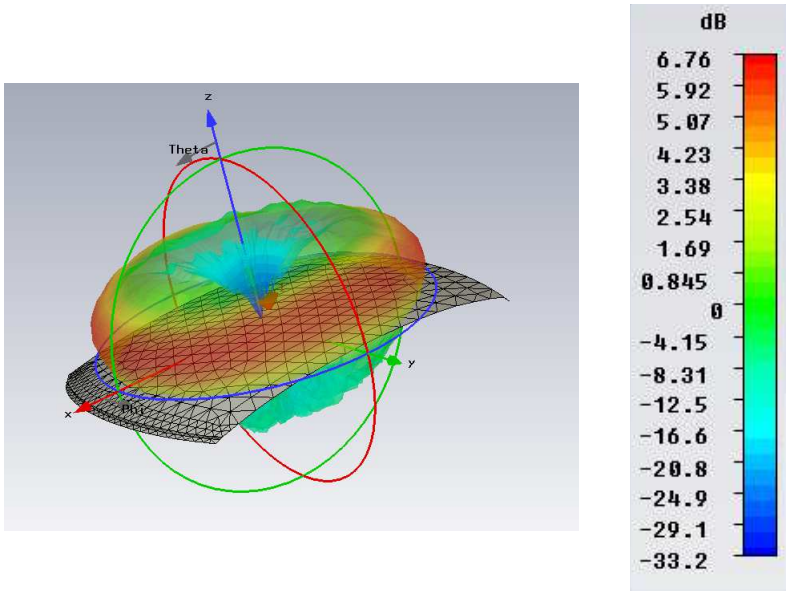

(a) Radiation pattern (b) Legend

Figure 5.8: 3D Radiation pattern of a dipole perpendicular to vehicle roof. Linear polarization in θ direction.

Frequency (GHz)	λ**(mm)**	***Hw***	***Hp***	**Material**
2	150	10λ	7λ	PEC

Table 5.5: Vehicle roof characteristics.

To study the vehicle roof with its curved structure, two more simulations of curved planes are done. Both simulations are compared with the circular plane Rp equal to 10λ to see the differences between the effect of a flat and a curved plane. One plane is chosen with a slight curvature and the other with a extreme one, moreover they follow the same sketch as shown in Figure 4.8 and 5.2 so that the areas are equal over the shape. The variable Tp is considered equal to 6.4 mm along all.

The aim is to compare both curvatures with the circular flat plane to show the trend in the radiation diagram produced by curved planes. First of all, a 3D radiation pattern of a slightly curved plane is shown in Figure 5.9. The plane diameter is 20λ so that it can be compared with a circular plane of Rp equal to 10λ. Secondly, a 3D radiation pattern of an extreme curved plane is shown in Figure 5.10. If the 3D radiation patterns are observed, it seems that when there is more curvature the inclination θ of the radiation pattern maximum decreases according to the curvature. Thus, the radiation seems to be more spread out along the surface.

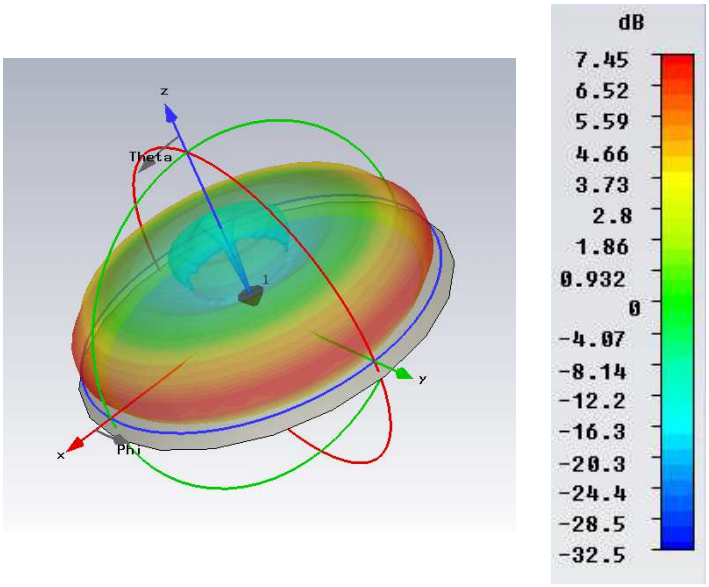

(a) Radiation pattern (b) Legend

Figure 5.9: 3D Radiation pattern of a dipole perpendicular to a slightly curved conducting plane. Linear polarization in θ direction.

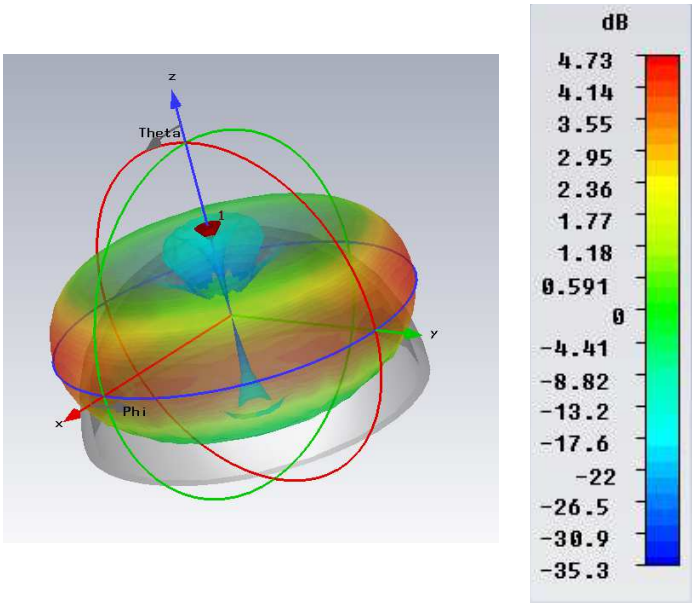

(a) Radiation pattern (b) Legend

Figure 5.10: 3D Radiation pattern of a dipole perpendicular to an extreme curved conducting plane. Linear polarization in θ direction.

As seen in the previous figures, the radiation seems to be more spread out over the curved

surface. The inclination of the radiation decreases according the surface. Therefore, in this case, the diffraction effect changes. As the surface is curved, not all the waves arrive directly to the discontinuity, obviously this depends on the grade of curvature of the surface. In case of a very extreme curvature as for example Figure 5.10, the edges are in the bottom of the structure. Thus, the waves do not reach directly the edges, so it seems that the radiation pattern will not be affected by the diffraction effect [23] and in consequence the shape will be smoother. The comparison among the curved planes and the circular plane is shown in Figure 5.11 and their characteristics are given in Table 5.6. It is observed that the curvature of the planes has a considerable influence on the radiation pattern [24][25]. The radiation pattern of the circular plane corresponding to a Rp equal to 10λ and the slightly curved plane are represented by red and blue colour respectively. If both are observed, there are two clear differences between them. It seems that when the plane is slightly curved, the trend is to decrease the inclination of the main lobe of the radiation pattern and somehow to spread out the radiation in all directions [6]. If the curvature is extreme as in the simulation represented by pink colour, the effect of the spread out radiation becomes clearer. The main and lower side lobes are less distinguishable and in consequence the antenna is less directive as shown in Figure 5.11. Hence, the presence of very curved structures is not desirable in case a directive antenna is needed due to the fact that the effect of the curvature is to spread out the radiation. There is also less diffraction effect as the curvature grade is increased.

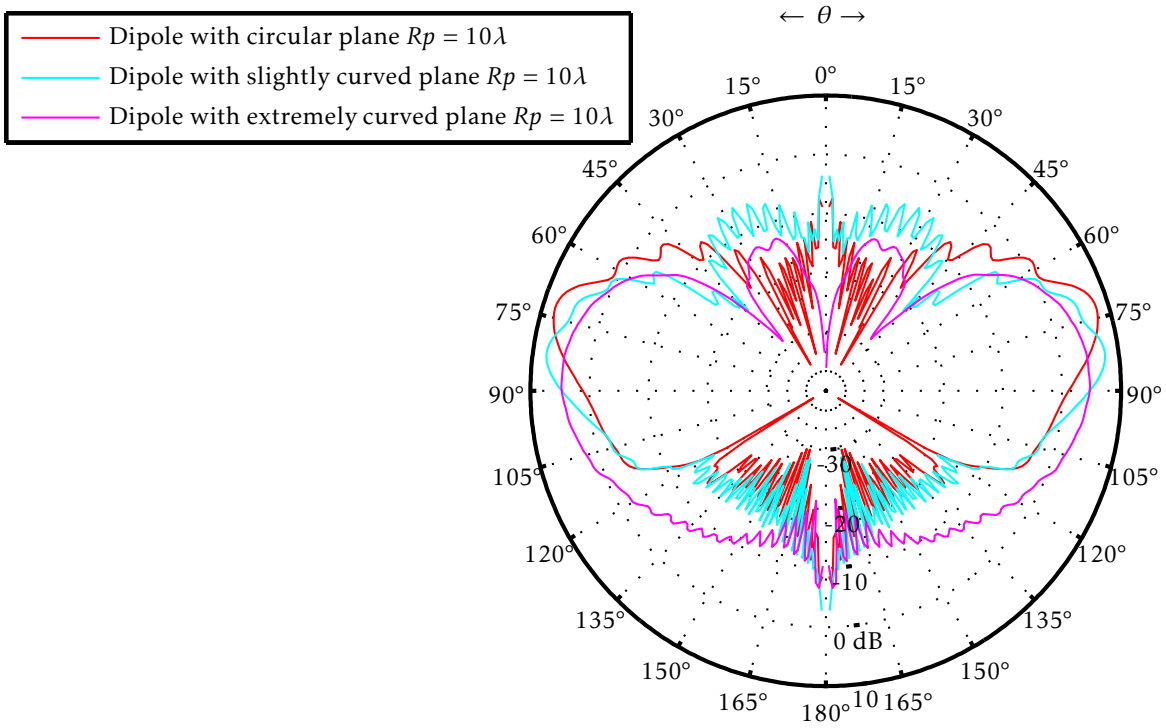

Figure 5.11: Gain in dB of a dipole perpendicular to a circular, slightly curved and extreme curved plane (θ, $\phi = 90°$).

Plane types	Main lobe direction (θ)	Main lobe magnitude	Angular width (-3dB)	Reflection coefficient S_{11}
Circular $Rp = 10\lambda$	73°	7.9 dB	16°	-7.12 dB
Slightly curved	82°	7.7 dB	19.2°	-7.75 dB
Extremely curved	89°	4.8 dB	37.2°	-5.32 dB

Table 5.6: Characteristics of the simulations shown in Figure 5.11.

Now, the vehicle roof is compared with the corresponding radius Rp equal to 5λ of the circular plane. The used vehicle roof is a mixture of a square plane due to the edge which corresponds to the plane width Hw, a circular plane due to the edge which corresponds to the plane height Hp and a curved plane due to its slight curvature. In Figure 5.12 the comparison between the vehicle roof and the circular plane is shown. The corresponding simulation characteristics are also given in Table 5.7.

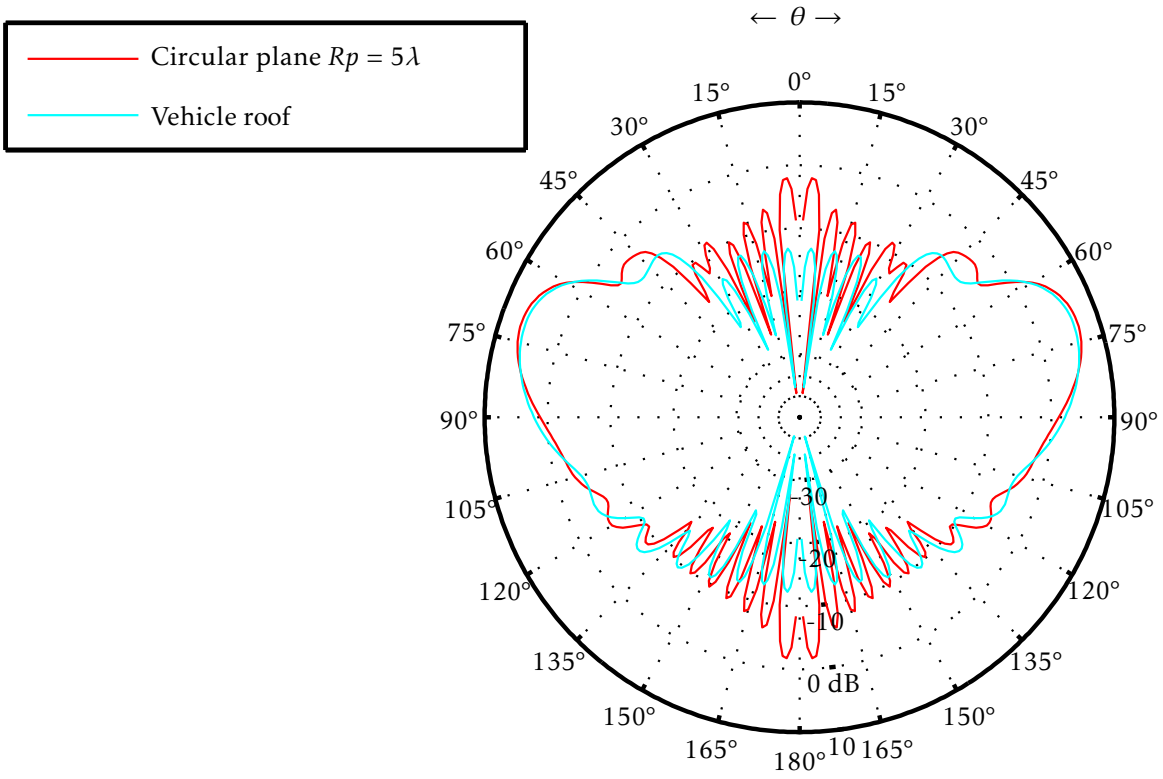

Figure 5.12: Gain in dB of a dipole perpendicular to a circular plane and the vehicle roof (θ, $\phi = 90°$).

Plane types	Main lobe direction (θ)	Main lobe magnitude	Angular width (-3dB)	Reflection coefficient S_{11}
Circular $Rp = 5\lambda$	73°	7.9 dB	16°	-7.12 dB
Vehicle roof	72°	6 dB	26.8°	-7.15 dB

Table 5.7: Characteristics of the simulations shown in Figure 5.12.

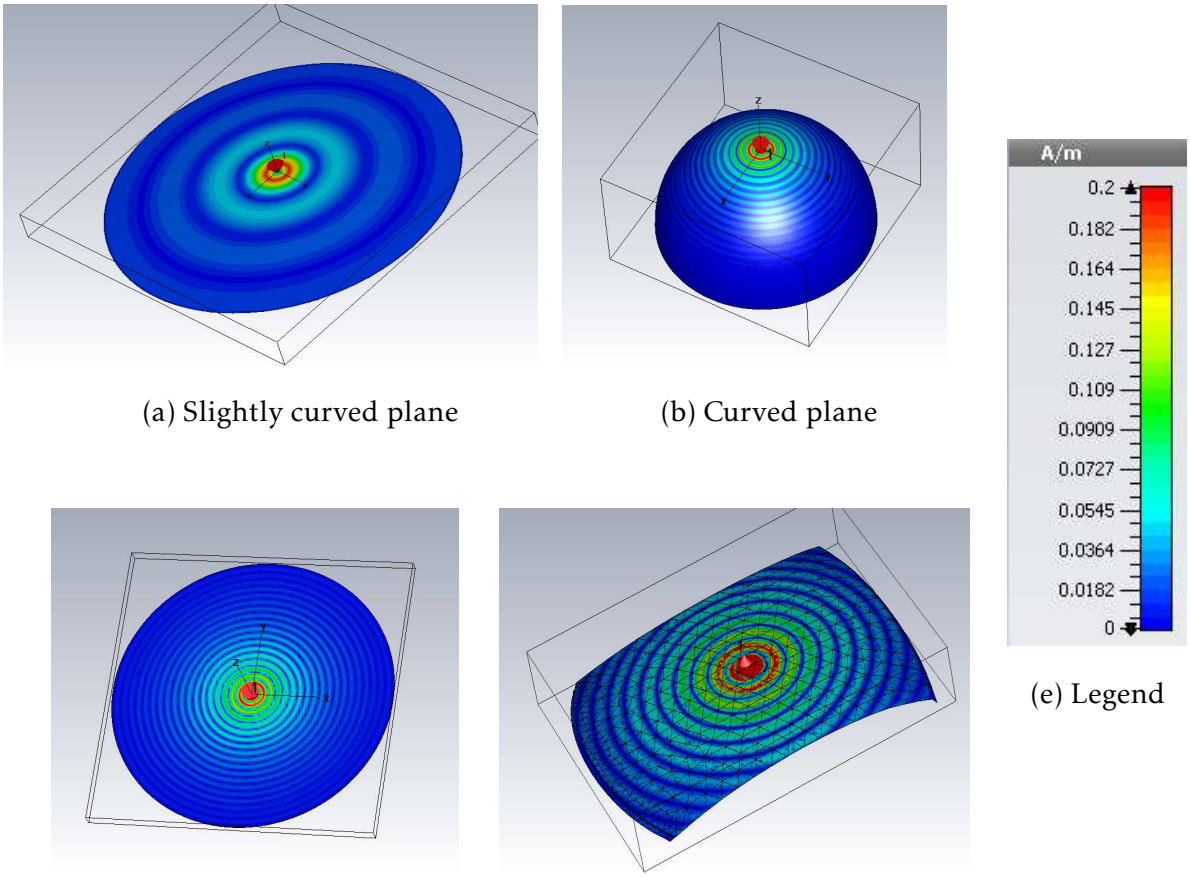

(a) Slightly curved plane

(b) Curved plane

(c) Circular plane

(d) Vehicle roof

(e) Legend

Figure 5.13: Surface currents corresponding to different curved planes.

As can be seen in Figure 5.12, if the plane size is Hw and Hp equal to 10λ, the radiation pattern can not be considered as the radiation pattern which an infinite plane would produce. In case of the vehicle roof represented by blue colour, its size corresponds to a plane edge Hw and Hp equal to 10λ which is not equal to the threshold commented in Subsection 5.1.1. It seems that the radiation pattern is improved in some aspects comparing to the circular

plane of Rp equal to 5λ which is represented by red colour. The side lobes of the vehicle roof become weaker and the radiation is not very spread out due to the curvature of the vehicle roof. Therefore, considering the case of the vehicle roof, it can be seen that having a curved plane with a straight and curved edges combined, has provided an improvement on the radiation pattern because this fact reduces the diffraction effects. Hence, the curvature in the vehicle roof has not a considerable influence, even in this case seems to make the side lobes weaker. In addition, the influences of the diffractions are also considerable, but considering the whole vehicle, the edge length will be greater than the threshold and the diffraction effect will be lower.

Finally, the surface currents for the circular plane, slightly and extremely curved planes and the vehicle roof are shown in Figure 5.13. The surface currents of the slightly and extremely curved plane are minor than 0.25% of the dipole current maximum. This is because the plane diameter in both cases is equal to 20λ so that it reaches the threshold. However, the vehicle roof size is comparable to an edge length of Hw equal to 10λ and that is why the currents on it are higher than in the rest of cases. The edge lengths of the vehicle roof are Hw around about 10λ and Hp around about 7λ and as a consequence the conducting plane does not behave as an infinite one. In conclusion, the diffraction effect in the vehicle roof case is less than for the circular plane, moreover the curvature grade of it is slight which means that the lobes are slightly spread out. In general, the vehicle roof improves the radiation in comparison to a square plane.

5.1.3 Distance dipole-plane

In the following subsection, the effect on the radiation pattern due to the distance dipole-plane is investigated. Thus far, a fixed distance dipole-plane equal to 3.4 mm has been considered. However, the shape and magnitude of the field is not only influenced by the plane shape. There is another dependency on the distance dipole-plane and for this, five simulation for different Kp values are done and shown in Figure 5.14.

In [6], several simulations for different Kp values are shown. However in case of [6], the diffraction effects are not present due to the fact that is considered an infinitesimal electric dipole above an infinite perfect conductor. In Figure 5.14, a dipole of $\lambda/2$ above a finite square conducting plane is considered. The simulation represented by red colour corresponds to a value Kp around about $\lambda/40$, which was used in all the simulations shown until here. The edge length of the plane used for the simulations in Figure 5.14 corresponds to a Hw and Hp equal to 5λ because of the side lobes are clearer for this edge length.

The equation 4.1 is still valid for different Kd values. As commented in last chapters, the side lobes appears based on the edge length of the conducting plane. In Figure 5.14, all simulation are computed for a fixed edge length equal to 5λ. Therefore, it shows that as Kp is increased, the number of side lobes is the same and only the radiation is widened in all directions.

If the red simulation is compared to the blue one, the main lobe inclination plane decreases and the upper side lobes become wider. One step more, the simulation represented by pink colour, the main lobe inclination is decreased again, and the upper side lobes are joined.

If Kp is further increased as in the simulations represented by black and green colour, the trend is to join all the lobes in one as if the diagram pattern is the dipole one. This seems logical because the distance between the dipole and plane is larger and the plane effect should become weaker.

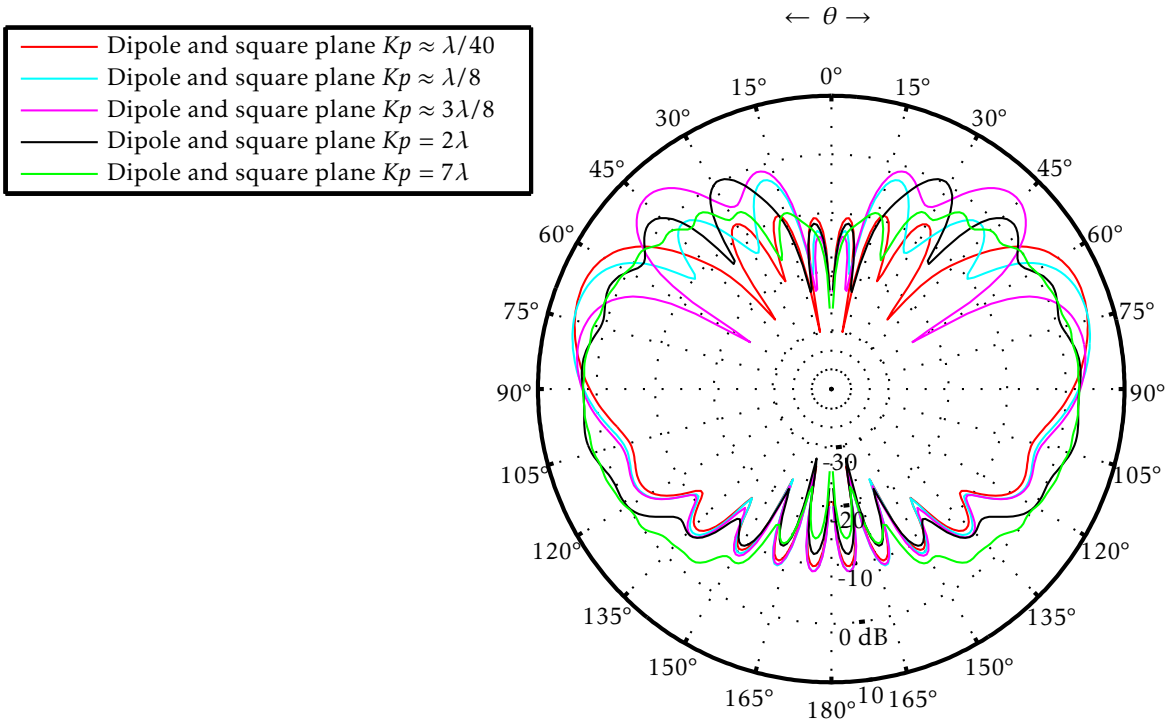

Figure 5.14: Gain in dB of a dipole perpendicular to a square plane of $Hw = Hp = 5\lambda$ for different Kp values (θ, $\phi = 90°$) at 2GHz.

5.2 Image theory verification

In the following section, the verification of the Image theory is investigated. Moreover, the corresponding effects of diffractions and the image theory are identified. As commented in Section 5.1.1, if the conducting plane is large enough, it can be approximate as an infinite one and the image theory can be applied then. In this case, the dipole (real source) and the conducting plane can be substituted by the real dipole and another dipole (virtual source) located co-lineally to it. The virtual dipole has to be at a distance equal to the double of Kp as shown in Figure 5.15. The values of Kp and L still the same as in the last sections, therefore Kp is equal to 3.4 mm and L is equal to $\lambda/2$. There is also the option to simulate an infinite plane in CST. For this purpose, a conducting wall has to be used by setting the boundary conditions to neglect the radiation downward it. However, in order to get comparable results with the square plane, the co-lineal dipoles need to be simulated.

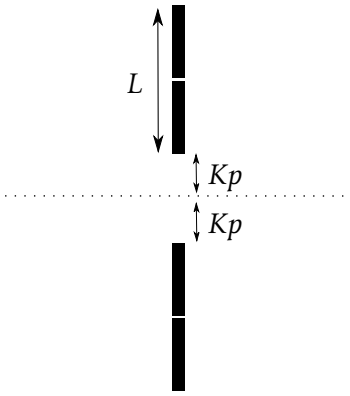

Figure 5.15: Sketch of co-lineal dipoles.

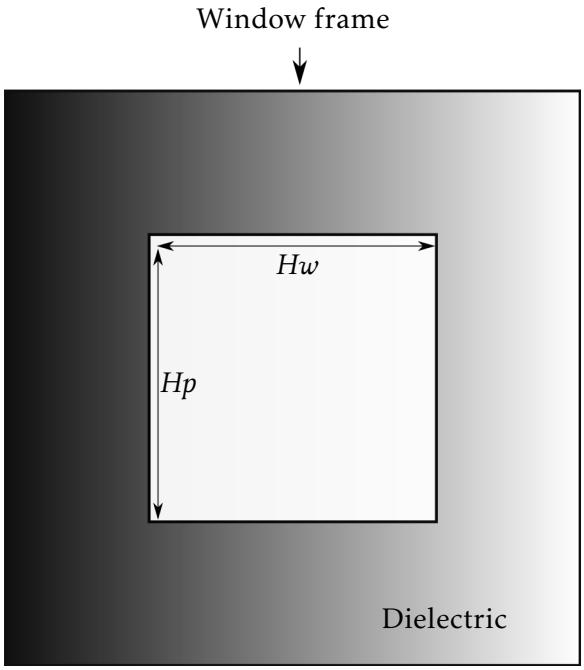

Figure 5.16: Sketch of the window frame.

If a dipole above a square plane is simulated, the radiation pattern produced by the dipole is only affected by the area of the square plane instead of an infinite plane. Thus, when the square plane is substituted by the virtual dipole, only the area corresponding to the square plane must be contributing to the radiation pattern. To do this, the co-lineal dipoles are placed symmetrically at the middle of a dielectric window frame. The window frame has a gap at its center equal to the edge lengths Hw and Hp equal to 20λ of the square plane as shown in Figure 5.16. The intention with this dielectric is to allow only radiation where the plane was and avoid the radiation beyond it. The 3D radiation pattern of the co-lineal dipoles perpendicular to the window frame is shown in Figure 5.17. To reach optimal results

the window frame made of dielectric material must be as large as possible, nevertheless due to the fact that the simulation takes too much time to be finished, the size of the frame has been reduced.

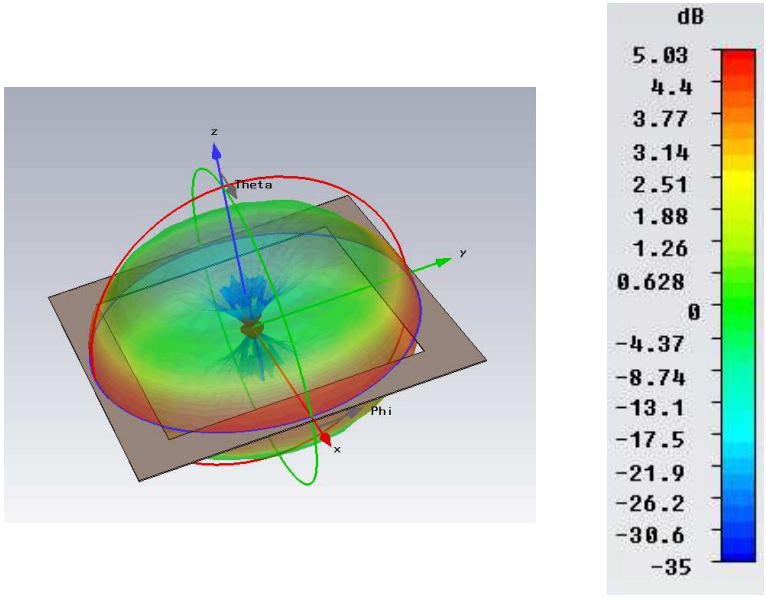

(a) Radiation pattern (b) Legend

Figure 5.17: 3D Radiation pattern of co-lineal dipoles perpendicular to a dielectric window frame. Linear polarization in θ direction.

In addition, in order to prove the effect of an infinite perfect conducting plane another simulation in CST is done using a conducting wall which actuate as an infinite plane. The 3D radiation pattern of the dipole perpendicular to the conducting wall is shown in Figure 7.9. The comparison among the co-lineal dipoles, the co-lineal dipoles perpendicular to the window frame, the square plane of Hw and Hp equal to 20λ and the dipole above an infinite conducting plane is shown in Figure 5.18. Additionally, the comparison between the co-lineal dipoles and the dipole with an infinite conducting plane is separated from the comparison between the co-lineal dipoles perpendicular to the window frame and the square plane as shown in Figure 7.7 and 7.8 respectively. These last comparisons are shown in order to distinguish easier the effects of each one.

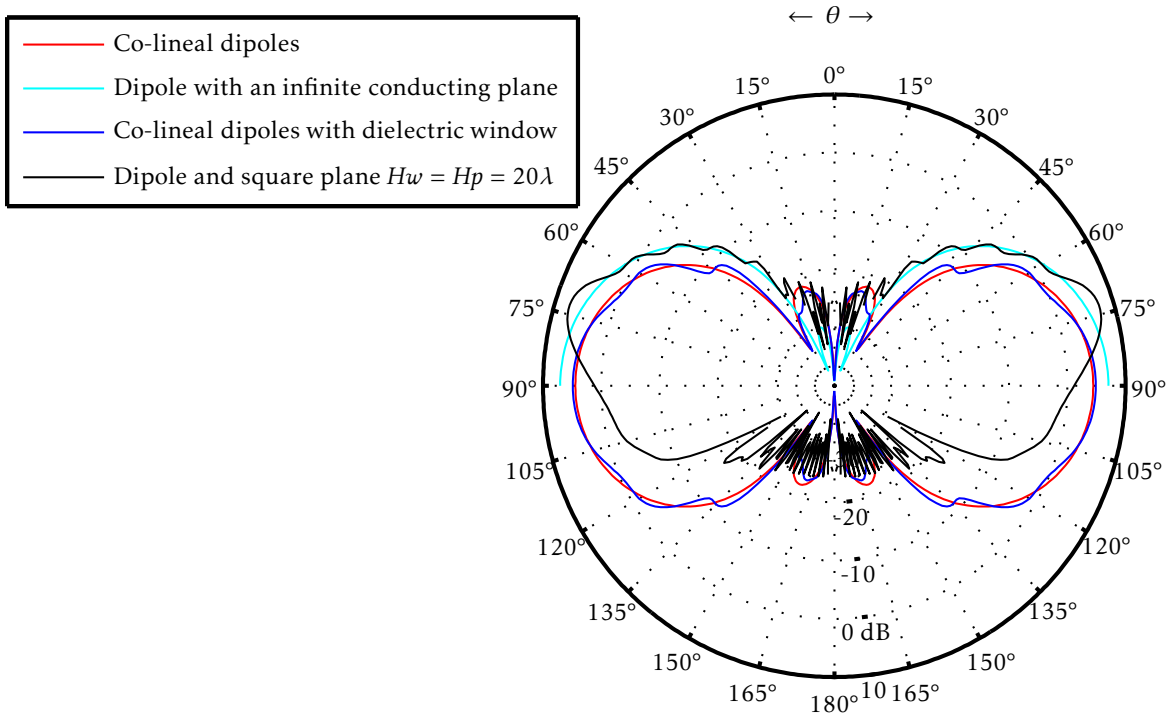

Figure 5.18: Gain in dB of co-lineal dipoles, dipole with a conducting plane, co-lineal dipoles with dielectric window and a dipole perpendicular to a square plane (θ, ϕ = 90 °) at 2 GHz.

The simulation represented by blue colour belongs to a dipole perpendicular to an infinite conducting plane using a conducting wall. In this case, the diffraction effects are not present due to the fact that there are no discontinuities, as for example corners and edges. Only the interaction of the radiation between the dipole and the infinite conducting plane is taken into account so that the radiation downward the conducting plane is cancelled. The radiation pattern is shaped with two main lobes and two weak secondary ones and only the half upper part of the radiation pattern is seen due to the fact that the infinite plane do not allow the radiation downward it as commented before.

The simulation represented by black colour belongs to a square plane of Hw and Hp equal to 20λ which was assumed in previous chapters as a good approximation to the infinite conducting plane. It is shown that the shape of the main lobe between θ equal to 0 ° and 60 ° follows approximately the same shape as in the simulation of a dipole with an infinite conducting plane represented by blue colour. There are only some differences as ripples and sharp secondary lobes due to the diffraction. Therefore, by comparing the simulation with the infinite plane represented by blue colour and the simulation of the square plane represented by black colour, it becomes clearer that the effect due to the diffraction is to corrugate and deform the lobes in a different way but keeping the same amount of radiation. Moreover, this deformation of the lobes increases the directivity of the antenna.

Another possibility for investigation, according to the image theory, is that a dipole image

can substitute a finite conducting plane so that there are two co-lineal dipoles. This simulation is represented by red colour and is shown in Figure 5.18. In order to approximate this case as the finite square plane, the window frame is introduced. With it, simulation represented by dark blue colour, the result should be approximately the same as the simulation of the dipole with the square plane. Therefore, if the square plane is considered, the conducting plane produces reflected and diffracted waves. However, following the image theory and using the dielectric windows frame to make comparable both cases, the resulting radiation pattern is not exactly the same because the dielectric window should be infinite and this fact is not realizable. On the other hand, the dielectric window produces similar effects as the diffraction in the square plane but the fact that the conducting plane is not present the diffraction mechanism cannot reach the same behaviour. This means that the radiation of the radiation pattern cannot be redistributed as it should be.

Hence, the blue simulation represents exactly the effects of an infinite perfect conductor below a dipole of $\lambda/2$. The dark blue simulation represents the effect on the radiation pattern of a finite plane but following the image theory.

In conclusion, the diffraction effects are important because they produce the most significant changes on the radiation pattern. In case of the simulation of the dipole with the infinite plane, the diffraction effect is not present because there are no discontinuities. In addition, there is no radiation under the plane because there is no way to have diffraction under the conducting plane. In case of the simulation of co-lineal dipoles with the dielectric window, there is radiation in the lower part of the radiation pattern because the radiation is not cancelled because there is no physical plane. Moreover, the diffraction effect cannot be obtained for the same reason. However, limiting the area as if the square conducting plane would be there, the trend of the diffraction effect is glimpsed. Finally, two important effects can be distinguished. One is the shape change of the radiation pattern which is mainly influenced by the Image theory. On the contrary, if a shape of the radiation pattern due to the Image theory is given, the GTD produces the rest of changes on it. Due to the rays diffracted by the conducting plane, the main lobe is corrugate, side lobes are produced and the radiated energy is distributed in a different manner. This means that the lobes can be more or less directive and the inclination of the main lobe maximum changes.

5.3 Vehicle simulation

The vehicle model has been introduced in Chapter 4. It is composed by the vehicle structure and the front and back window. The effects of conducting environments have been always studied with the dipole located symmetrically at the center of the structure. The final dipole position is going to be at the back side of the vehicle roof, therefore the whole car with the real antenna position is going to be simulated and the front and back window are also taken into account.

5.3.1 Radiation pattern

First of all, the radiation pattern of the vehicle roof for the real antenna position and the antenna located at the center of the vehicle roof is compared in Figure 5.19. The 3D radiation

pattern of the vehicle roof and its characteristics are shown in Section 5.1.2. As can be seen in Figure 5.19 in red colour, when the dipole is located on the back side of the roof, the radiation pattern is no longer symmetric. This is due to the fact that the waves are not contributing to the radiation pattern symmetrically. As the antenna is located at one side of the vehicle roof, there are changes in the positions of the side lobes. This means that the diffracted rays from the closest edge from where the antenna is located, have more influence on the radiation pattern. Therefore they produces more ripples in the right side of the radiation pattern.

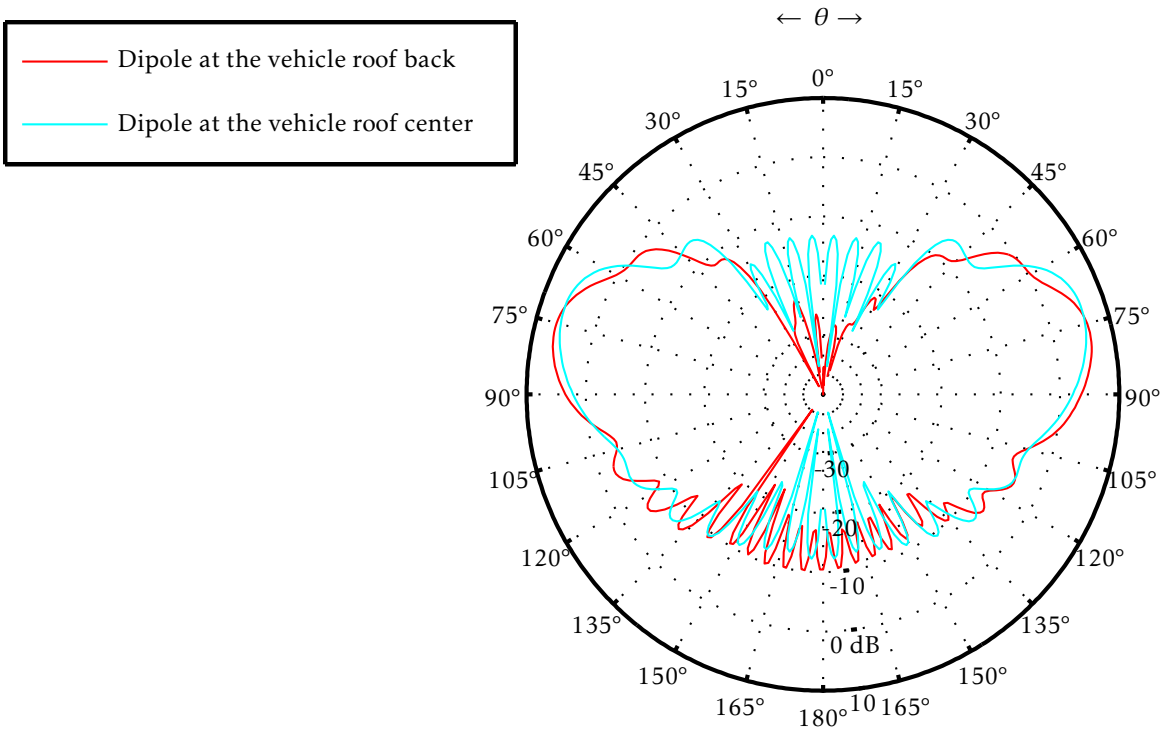

Figure 5.19: Gain in dB of a dipole above the center and the back side of the vehicle roof (θ, $\phi = 90°$).

From here, the antenna located above the back side of the vehicle roof is going to be considered. Despite the antenna is located above the right side of the vehicle roof, when the whole vehicle is considered, the radiation pattern becomes symmetrical again as can be seen in Figure 5.23. The 3D radiation pattern of the vehicle at 2 GHz is shown in Figure 5.20, also its sketch and characteristics are shown in Figure 5.21 and Table 5.8 respectively.

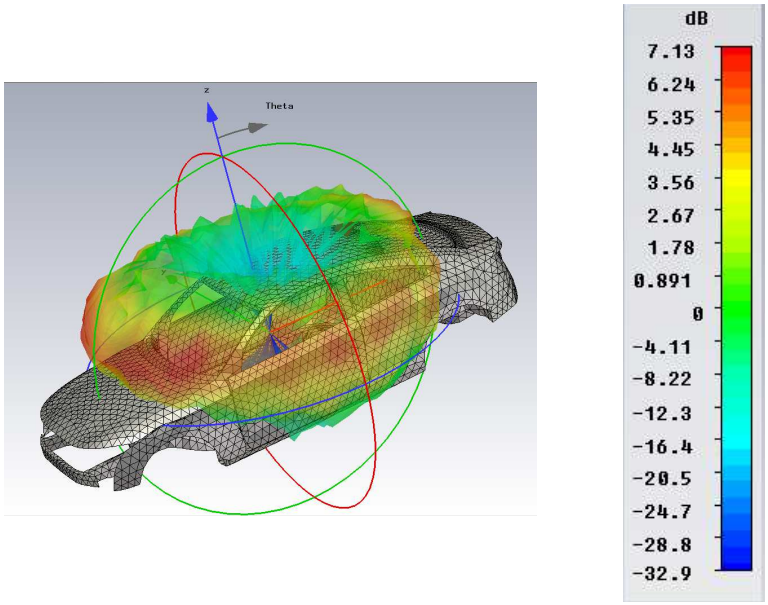

(a) Radiation pattern (b) Legend

Figure 5.20: 3D Radiation pattern of a dipole perpendicular to the vehicle roof. Linear polarization in θ direction.

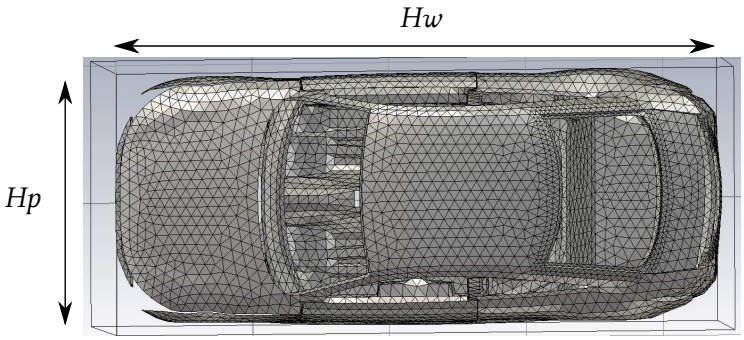

Figure 5.21: Sketch of the vehicle.

Frequency (GHz)	λ**(mm)**	***Hw***	***Hp***	**Material**
2	150	29λ	12λ	PEC

Table 5.8: Vehicle characteristics.

Now, several comparisons are done in order to identify the effects produces by the real vehicle structure. For this, the radiation pattern comparison between the vehicle and the

vehicle with windows is shown in Figure 5.22.

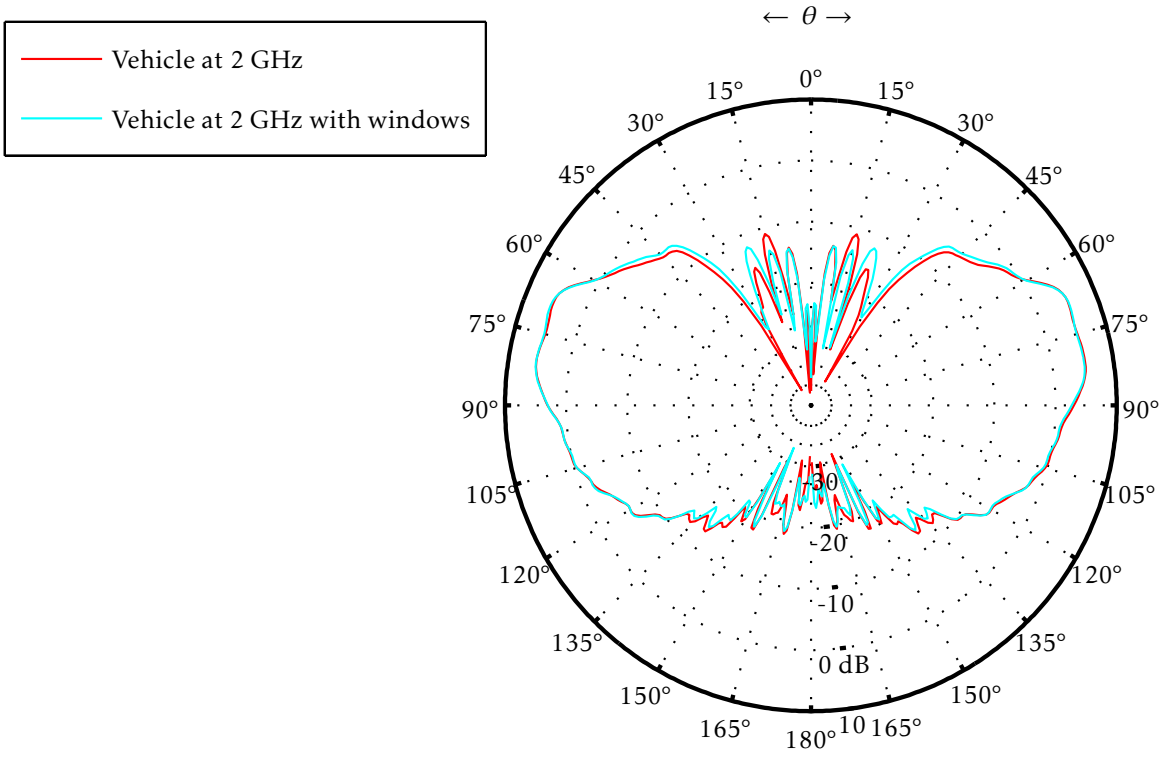

Figure 5.22: Gain in dB of a dipole above the vehicle and the vehicle with windows (θ, $\phi = 90°$).

The Figure 5.22 shows in red colour the radiation pattern of the vehicle without windows, and the blue colour represents the vehicle with windows. If both simulations are observed, the glass windows does not produce an important difference in the diagram pattern. The main lobes are practically equal, only the upper and lower side lobes differ. The magnitudes of the upper side lobes corresponding to the blue simulation are slightly different form the red one, but the magnitude does not surpass the maximum magnitude of it. Moreover, the lower side lobes are quite the same and the magnitudes are weak enough so that this can be ignored. For this reason, the vehicle without windows is taken into account from here. The 3D radiation pattern of the vehicle with windows at 2 GHz is shown in Figure 7.10 and its representation of the surface currents is shown in Figure 7.11.

Now, the simulation of the vehicle is compared with two important simulations. These simulation will allow to compare the vehicle and see in which way it is affecting the radiation pattern. For this, the comparison among the vehicle, the vehicle roof and the square plane of edge length Hw and Hp equal to 20λ is shown in Figure 5.23. The characteristics of each simulation are shown in Table 5.9. The comparison among the reflection coefficient of each simulation of Table 5.9 is shown in Figure 5.24. The reflected power into the port for the vehicle roof and the square plane simulation is about -7 dB. It is reflected more than 10%, however in case of the vehicle, the reflection coefficient is improved reaching a value of -8.2

dB.

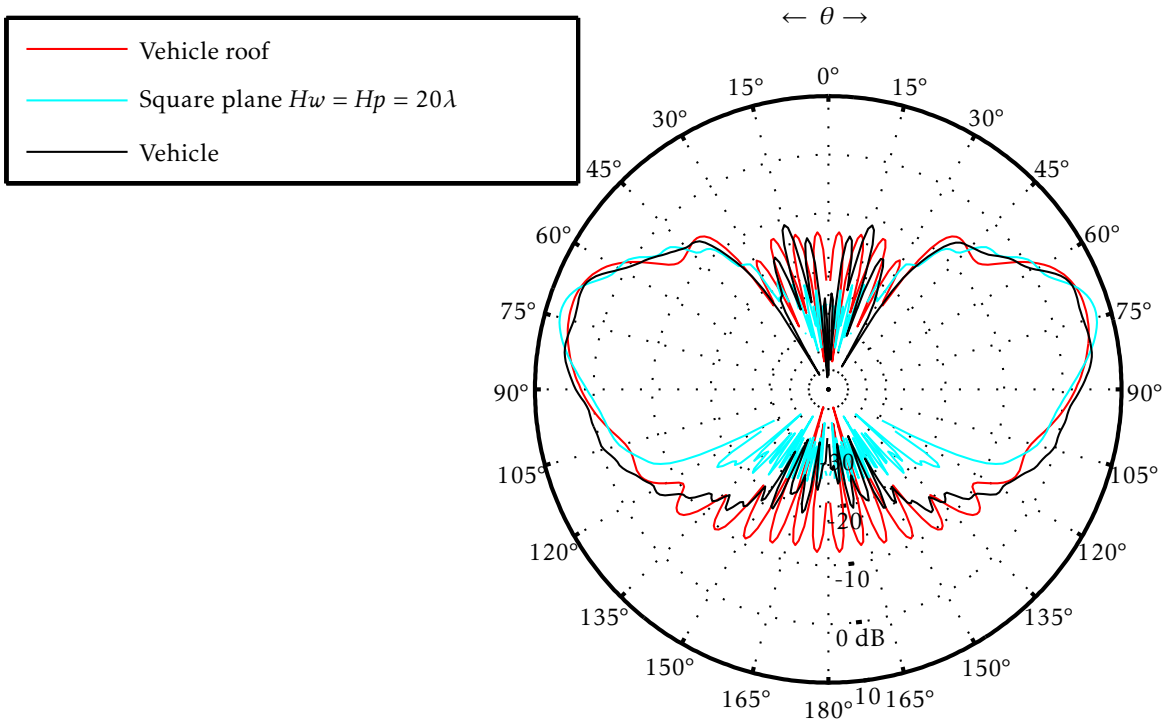

Figure 5.23: Gain in dB of a dipole above the vehicle, the center of the vehicle roof and a square plane of $Hw = Hp = 20\lambda$ (θ, $\phi = 90°$).

Structures	**Main lobe direction / magnitude**	**Angular width (-3dB)**	**Reflection coefficient** S_{11}
Vehicle roof with centered antenna	72°/ 6 dB	26.8°	-7.1 dB
Square plane *Hw* = *Hp* = 20λ	73°/ 7.5 dB	17.3°	-7.12 dB
Vehicle at 2 GHz	81°/ 5.9 dB	29.5°	-8.2 dB

Table 5.9: Simulation characteristics.

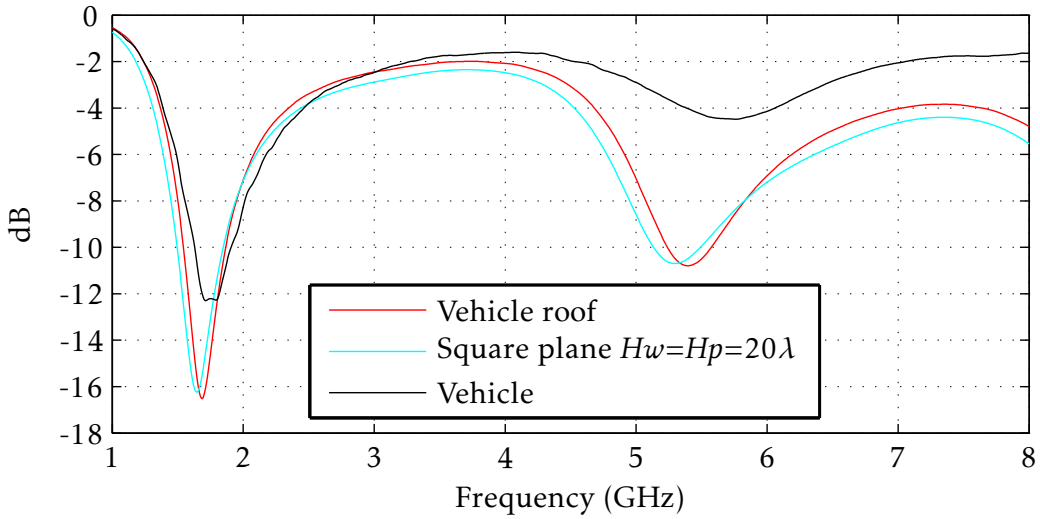

Figure 5.24: S_{11} parameter of the vehicle roof, the square plane of edge length equal to 20λ and the vehicle simulation for $Kd = 1.5$ mm at 2 GHz.

The diagram pattern of the square plane represented by blue colour is taken as a reference. Moreover, the vehicle roof simulation represented by red colour, is going to show the different effects between if the whole car and only the vehicle roof is taken into account. As commented in previous chapters, the optimal case is when the conducting plane has an edge length of Hw and Hp equal to 20λ. For this reason, the vehicle roof does not reach the optimal length due to the fact that its length is approximately 10λ. As a consequence, the radiation pattern of the vehicle roof is not as directive as the square plane and the side lobes are more intense. Considering the whole vehicle, a length larger than Hw equal to 20λ and Hp equal to 10λ is reached. If Figure 5.20 is observed, despite the antenna is located on the back side of the vehicle roof, more than only the vehicle roof is influencing the radiation pattern. Observing Figure 5.23, the upper part of the main lobe corresponding to the vehicle simulation and represented by black colour is similar to the main lobe of the blue simulation corresponding to the square plane. Only the lower side lobes and the lower part of the main lobe differ considerably between them. Hence, three trends can be identified in the vehicle simulation according to the last chapters.

The first of the characteristic changes in the far-field pattern is about the shape of the main lobe. As commented before about the vehicle simulation, the upper part of the main lobe is very similar to the optimal case corresponding to the square plane of Hw and Hp equal to 20λ. There are few different distortions on the main lobe due to the diffraction effect. Moreover, the vehicle structure simulated is more complex than the square plane due to the fact that it is formed by the joining of various pieces. Therefore, in case of the vehicle, the diffractions are produced in each discontinuity of each piece.

The second of the characteristic changes in the far-field pattern is about the magnitude of the upper side lobes. As the edge length Hp does not reach the optimal length of 20λ, the magnitude of the side lobes is higher than the side lobes of the square plane. As commented

in last chapters, as the edge length of the structure is increased, more side lobes appears with less magnitude. If both edge lengths of the vehicle simulation were equal, the side lobes would be comparable to the square one. In addition, the shape of a vehicle tends to be more curved than straight, therefore the edges create caustics and these entail to more intense side lobes.

Finally, the third of the characteristic changes in the far-field pattern is about the curvature. As the dipole is located on the back side of the vehicle roof, the diagram pattern is affected by the back side of the whole vehicle too. This implies as the back side of the vehicle has a very curved structure, the radiation pattern is considerably spread out. In other words, the lower side lobes are less distinguishable and seem to join each other. In addition, if the three simulations are compared, the side lobes of the vehicle simulation are not as intense as in the vehicle roof simulation but not as weak as the square case. This is because the vehicle size in near to the optimal case so that the side lobes magnitude need to be minor than for the vehicle roof. However, due to the fact that there is a considerable curvature in the vehicle structure, the radiation pattern resulting is more spread out over the surface. As commented in last chapters, the curvature tends to widen the radiation and to join the side lobes. At the end, the resulting radiation pattern changes according to the combination of the structure size, the curvature of the structure, if there are curved edges or not and the position of the dipole above the conducting structure. Therefore, all this considerations have to be taken into account, depending on the interests.

In conclusion, the approximations and reductions which have been defined along the study seem to be well considered. After this study, when complex conducting environments have to be analysed, the effects produced by the conducting environment can approximately be expected and anticipated.

5.3.2 Surface currents

Finally, the surfaces currents on the vehicle are shown in order to see which parts of the vehicle affects the radiation pattern. The representation of the surface currents corresponding to the vehicle at 2 GHz is shown in Figure 5.25.

As can be seen, the dipole is located above the back side of the vehicle roof. The high magnitudes of the current cover parts of the vehicle roof and the back side of the vehicle. In the rest of it, the surface currents are equal to 0. As was expected before, the resulting radiation pattern of the dipole above the vehicle showed that the dominant effects on it were the curvature of the back side of the vehicle because the dipole is located on the back side of the vehicle roof and the half right part of the vehicle roof. The surface currents on the vehicle can be found exactly on those parts.

In conclusion, the current magnitude in almost all the structure of the vehicle is minor than the 0.25% of the maximum current of the dipole and only in part of the vehicle roof and the back side of the vehicle corresponding to an approximately length of Hw equal to 10λ, the current magnitude is greater than the 2.5%. Once more, the surface currents indicates that not all the conducting structure affects the radiation pattern, there is a threshold from which an optimal result can be assumed.

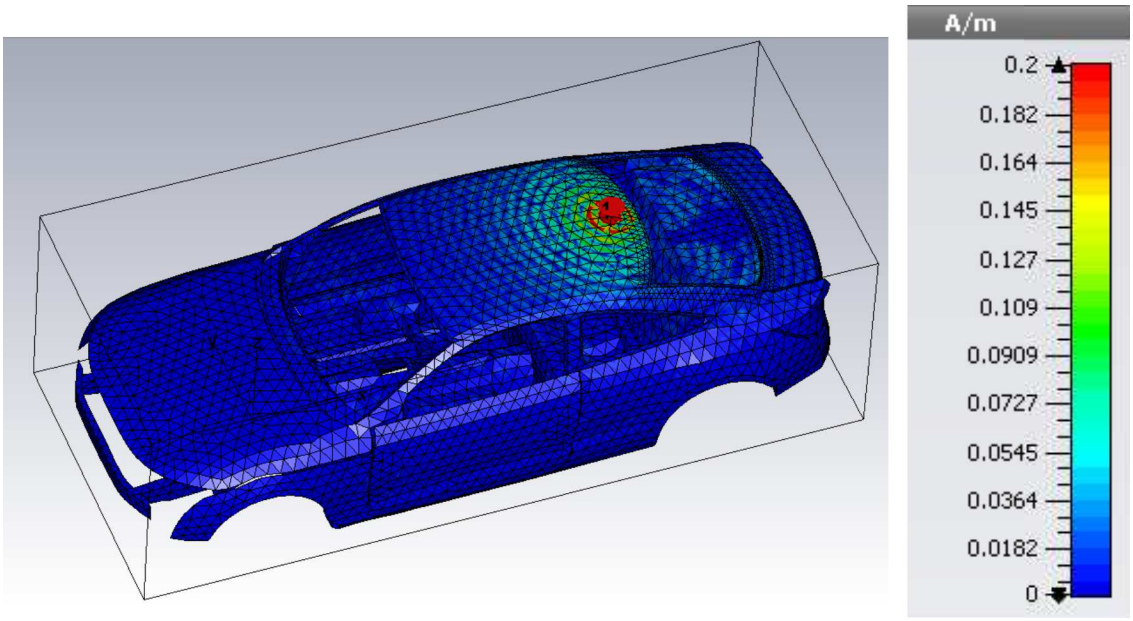

(a) Vehicle currents (b) Legend

Figure 5.25: Surface currents corresponding to the vehicle simulation.

6 Summary and outlook

The aim of the present research work was to study the influences of conducting environments on the radiation pattern of an antenna. The model under study is a vehicle structure with the antenna located above the back side of the vehicle roof.

First of all, some simplifications of the vehicle and the antenna were considered in order to reduce the simulation time. To study the influences of conducting environments on the radiation pattern, particular cases were considered each time to investigate its influences separately. Therefore, the first structure considered was a flat finite square plane in order to study the influences of corners and edges. The results showed that over certain structure size, the effects of the square conducting plane were minimal. Then, a second flat structure with circular edges was investigate to show the differences between straight and circular edges. It was shown that a circular edge has a different behaviour in respect to the square plane because of the caustics, which are points where several waves pass through them and in consequence the radiation is more intense. Thus, other simulations of plane shapes were investigated and compared with the previous square and circular results. The comparison on the one hand showed that the effects in the diagram pattern due to the different plane shapes, are the same independent of the plane shape if the plane shape is large enough. On the other hand, those effects could be explained by the GTD and Image Theory. Thus, the diffraction and reflection effects were introduced and some thresholds were found for the plane size.

The vehicle structures are normally curved, so that also the effect of curved plane was investigated. It was shown that the curvature has an important influence on the radiation pattern. The main effect of curved structures was to spread out the radiation according to the curved surface. Moreover, other structure attributes were investigated, as for example the distance between the dipole and the conducting plane. As could be expected, increasing this distance, the effect of the conducting plane became weaker.

Additionally, the Image Theory was investigated in order to prove the validity of it and to differentiate the effects between it and GTD. For this, several simulations were done following the theory so that two co-lineal dipoles were simulated perpendicular to a dielectric window frame. Also the case of an infinite PEC was simulated using a conducting wall which CST interprets as an infinite plane. It was shown that Image Theory is a correct explanation of the radiation pattern when an antenna is close to a conducting plane and GTD effects can be neglected. Therefore, it was differentiated the GTD effects due to the plane discontinuities from the reflection effect. It was shown that the diffraction effect tends to modify the radiation pattern distribution. The diffracted waves tend to produce ripples on the radiation pattern shape and sharp side lobes.

Finally, the vehicle structure was studied and simulated. Taking into account all the previous results, the effects produced by the vehicle could be approximately expected.

The next steps should be to verify some of the most important simulations by measurements. Also some further simulations with horizontal aligned dipoles or directive antennas should be done to see if the observed effects can be confirmed. These simulations can also be used to verify if the time domain solver in CST MWS is the most appropriate one for such problems or if the results could be computed more efficient with other solvers.

7 Appendix

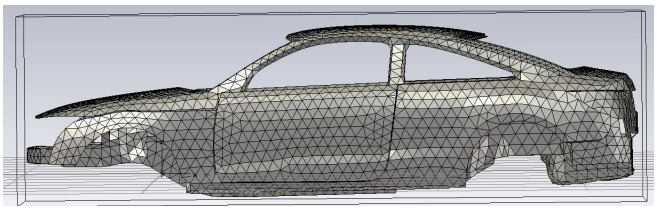

(a) View of the vehicle lateral.

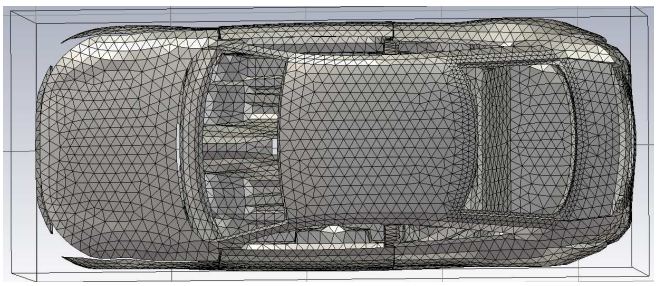

(b) View of the vehicle from above.

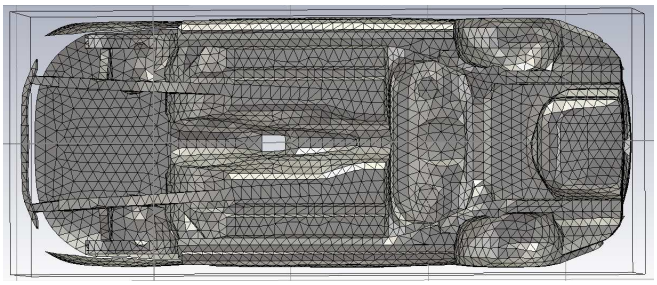

(c) View of the vehicle from below.

Figure 7.1: Vehicle views.

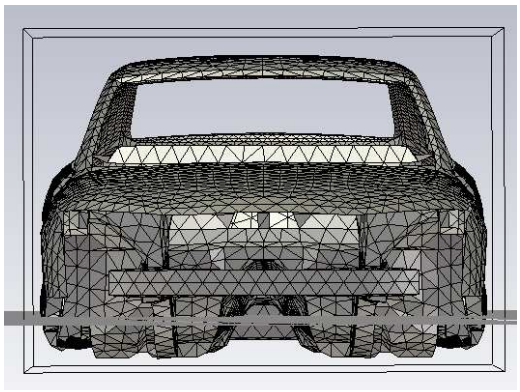

(a) View of the vehicle front.

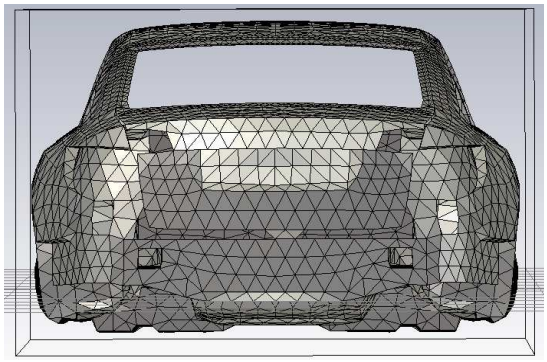

(b) View of the vehicle back.

Figure 7.2: Front and back view of the vehicle.

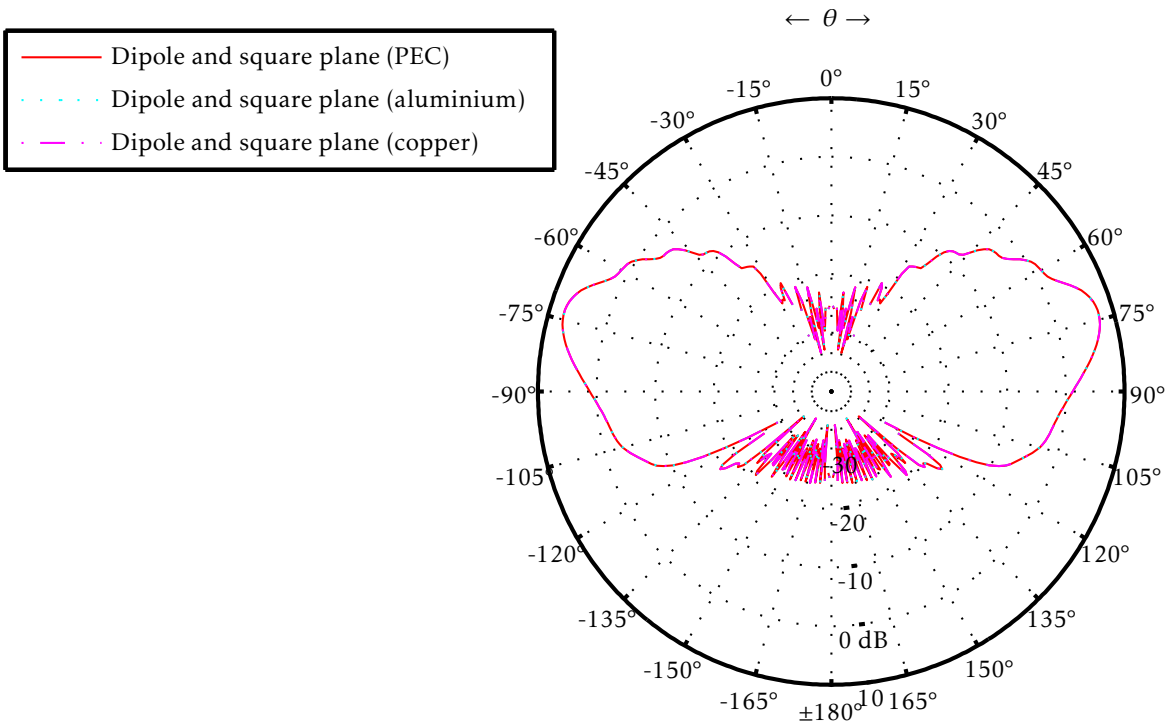

Figure 7.3: Gain in dB of a dipole perpendicular to a square plane of $Hw = Hp = 20\lambda$ for different materials (θ, $\phi = 90$ °).

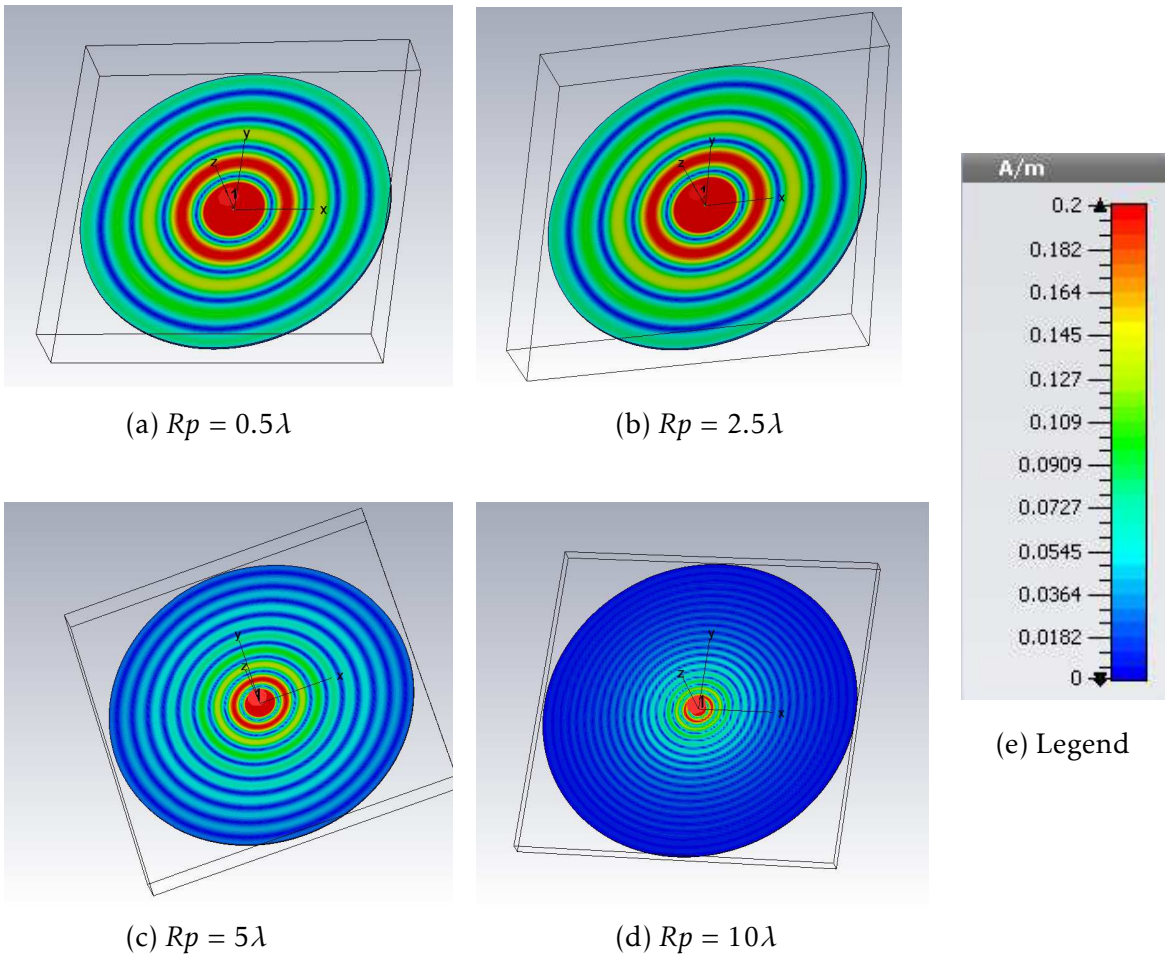

(a) $Rp = 0.5\lambda$ (b) $Rp = 2.5\lambda$

(c) $Rp = 5\lambda$ (d) $Rp = 10\lambda$

(e) Legend

Figure 7.4: Surface currents corresponding to the different edge lengths of the circular conducting plane.

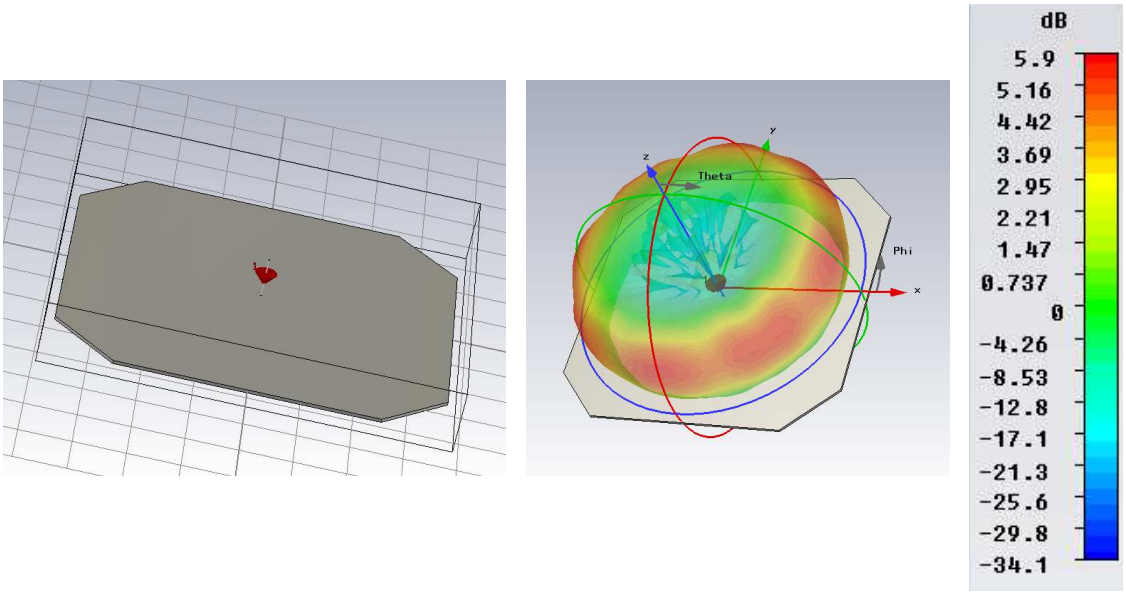

(a) Structure (b) Radiation pattern (c) Legend

Figure 7.5: Octagonal plane and its corresponding 3D radiation pattern for a edge length of $Hw = Hp = 5\ \lambda$.

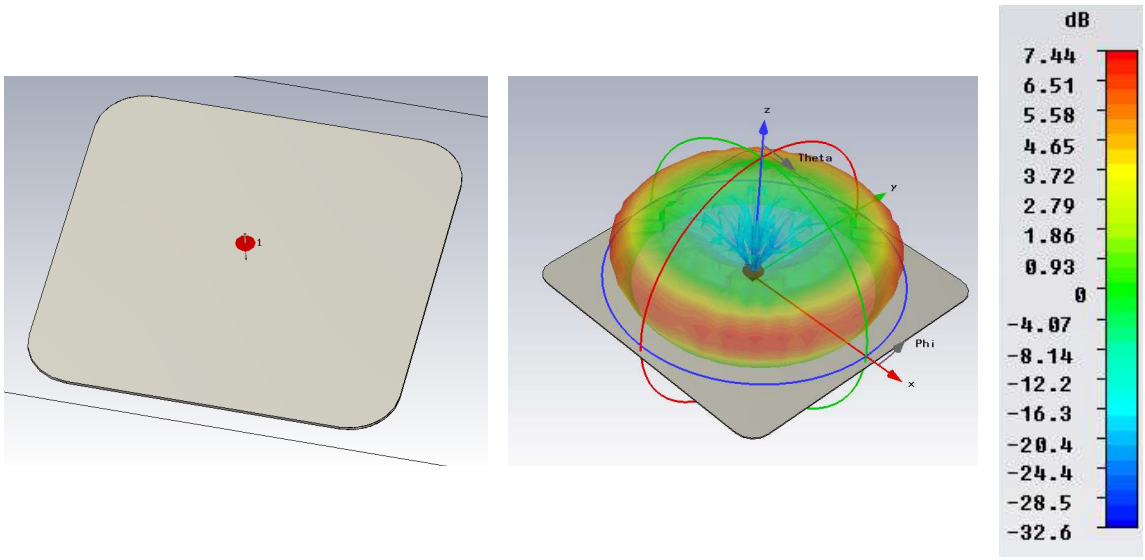

(a) Structure (b) Radiation pattern (c) Legend

Figure 7.6: Bended plane and its corresponding 3D radiation pattern for a edge length of $Hw = Hp = 10\ \lambda$.

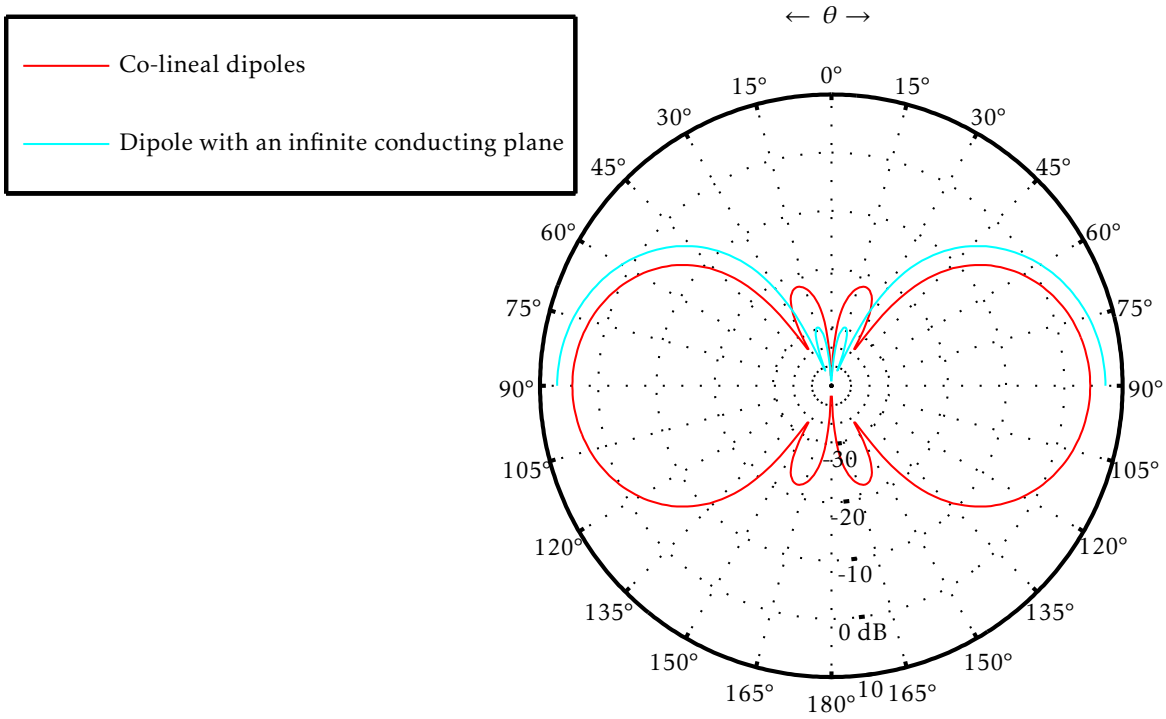

Figure 7.7: Gain in dB of co-lineal dipoles and dipole with a conducting plane (θ, $\phi = 90\,°$) at 2 GHz.

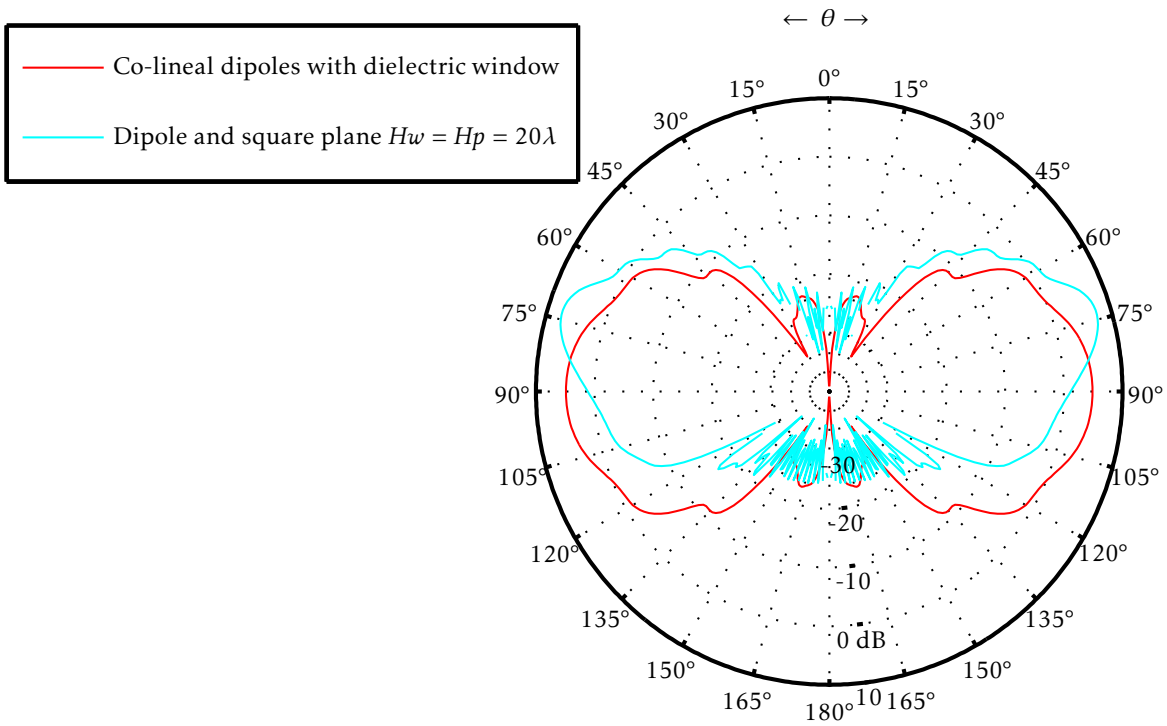

Figure 7.8: Gain in dB of co-lineal dipoles with dielectric window and a dipole perpendicular to a square plane (θ, ϕ = 90 °) at 2 GHz.

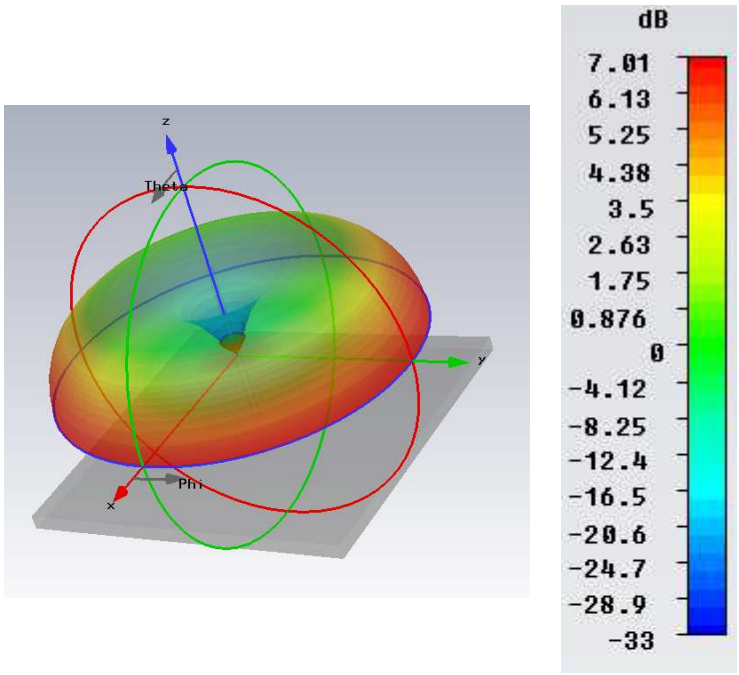

(a) Radiation pattern (b) Legend

Figure 7.9: 3D Radiation pattern of a dipole above a infinite conductor plane. Linear polarization in θ direction.

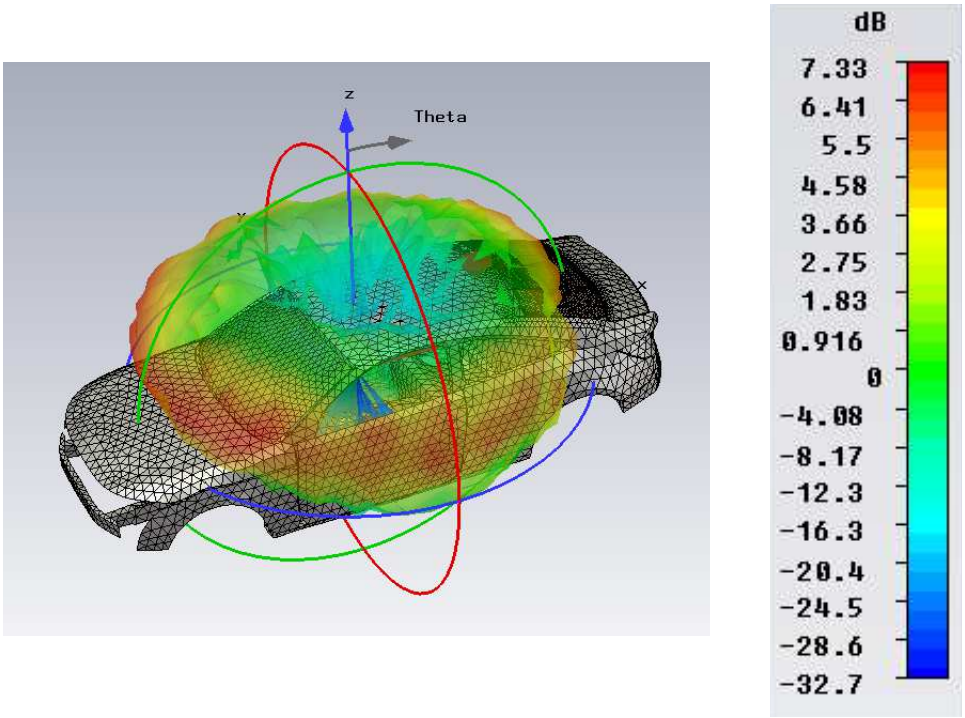

(a) Radiation pattern (b) Legend

Figure 7.10: 3D Radiation pattern of a dipole perpendicular to the vehicle with window. Linear polarization in θ direction.

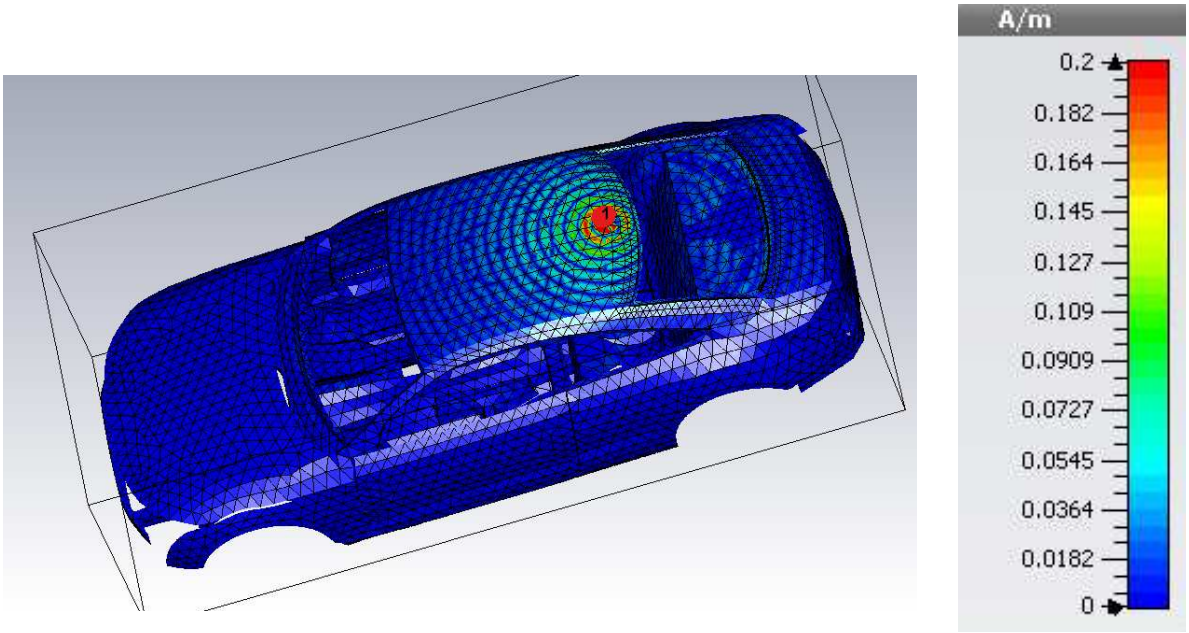

(a) Vehicle currents (b) Legend

Figure 7.11: Surface currents corresponding to the simulation of the vehicle with window.

Bibliography

[1] Guglielmo Marconi. Website: http://en.wikipedia.org/wiki/Guglielmo_Marconi.

[2] Hicham Tazi. *Disseration, Integration of Numberical Simulation Approaches in the Virtual Development of Automotive Antenna Systems*.

[3] CST Microwave Studio - Computer Simulation Technology. Website: http://www.cst.com/.

[4] EMCoS Consulting and Software. Website: http://www.emcos.com/Home.

[5] ANSYS HFFS. Website: http://www.ansys.com/.

[6] Constantine A. Balanis. *Antenna theory, analysis and design*. John Wiley and Sons, Inc., 3. edition, 2005.

[7] Constantine A. Balanis. *Advanced Engineering Electromagnetics*. John Wiley and Sons, Inc., 3. edition, 1989.

[8] Kraus Marhefka. *Antenna for all applications*. McGraw-Hill Companies, Inc., 3. edition, 2003.

[9] Peter Russer. *Electromagnetics, microwave circuit and antenna design for communications engineering*. Artech House, Inc., 2. edition, 2006.

[10] Daniel Fleisch. *A Student's Guide to Maxwell's Equations*. Cambridge University Press., 1. edition, 2009.

[11] L. I. Williams Y. Rahmat-Samii and R. G. Yoccarino. The UCLA Bi-Polar Planar-Near-Field Antenna Measurement and Diagnostic Range. *IEEE Antennas and propagation magazine*, Vol. 37(No. 6), December 1995.

[12] Antennas webpage of Universidad Politécnica de Valencia. Website: http://www.upv.es/antenas/ ©Miguel Ferrando, Alejandro Valero, Héctor Esteban. Comunications Depart. Universidad Politécnica de Valencia.

[13] Y.Y. Hu. A method of determining phase center and its applications to electromagnetism horns. *J. Franklin Inst.*, Vol. 271:31–39, January 1961.

[14] M. Teichman. Determination of horn antenna phase center by edge diffraction theory. *IEEE Trans. Aerospace Electr. Systems*, Vol. AES-9:875–882, November 1973.

[15] W. Kunysz. Antenna Phase Center Effects and Measurements in GNSS Ranging Applications. *14th International Symposium on ANTEM and the AMEREM*, 2010.

[16] D. Carter. Phase Centers of Microwave Antennas. *IRE Trans. Antennas and Prop.*, Vol. AP-4:597–600, October 1956.

[17] J. D. Dyson. "Determination of Phase Center and Phase Patterns of Antennas" in Radio Antennas for Aircraft and Aerospace Vehicles. *W. T. Blackband (ed.), AGARD Conference Proceedings*, (No. 15), 1967.

[18] J. B. Keller. Geometrical Theory of Diffraction. *J. Opt. Soc. Amer*, Vol. 52:116–130, February 1962.

[19] Alfred R. Lopez. The geometrical theory of diffraction applied to antenna pattern and impedance calculations. *IEEE Trans. Antennas and Propagat.*, Vol. AP-14(No. 1):40–45, January 1966.

[20] J. E. Storer. The radiation pattern of an antenna over a circular ground screen. *J. Appl. Phys*, Vol. 23:558, May 1952.

[21] R. G. Kouyoumjian and P. H. Pathak. A Uniform Geometrical Theory of Diffraction for an Edge in a Perfectly Conducting Surface. *Proc. IEEE*, Vol. 62(No. 11):1448–1461, November 1974.

[22] C. R. Cockrell and P. H. Pathak. Diffraction theory techniques applied to aperture antennas on finite circular and square ground planes. *IEEE Trans. Antennas and Propagat.*, Vol. AP-22(No. 3):443–448, May 1974.

[23] P. H. Pathak and R. G. Kouyoumjian. An Analysis of the Radiation from Apertures on Curved Surfaces by the Geometrical Theory of Diffraction. *Proc. IEEE*, Vol. 62(No. 11):1438–1447, November 1974.

[24] J. R. Wait and A. M. Conda. Pattern of an Antenna on a Curved Lossy Surface. *IRE Trans. Antennas Propagat.*, Vol. AP-6(No. 4):348–359, October 1985.

[25] P. Bechmann and A. Spizzichino. The Scattering of Electromagnetic Waves from Rough Surfaces. *Macmillan*, New York 1963.

[26] R. F. Harrington. *Field Computation by Moment Methods*. Macmillan Co., 1. edition, New York, 1968.